

C–H Bond Activation by Cationic Platinum(II) Complexes: Ligand Electronic and Steric Effects

H. Annita Zhong, Jay A. Labinger,* and John E. Bercaw*

Contribution from the Arnold and Mabel Beckman Laboratories of Chemical Synthesis, California Institute of Technology, Pasadena, California 91125

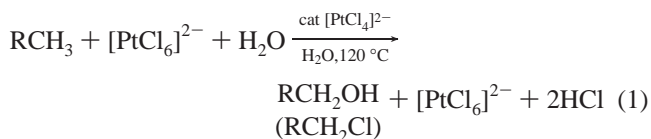
Received May 14, 2001

Abstract: A series of bis(aryl)diimine-ligated methyl complexes of Pt(II) with various substituted aryl groups has been prepared. The cationic complexes $[(ArN=CR-CR=NAr)PtMe(L)]^+[BF_4]^-$ (Ar = aryl; R = H, CH₃; L = water, trifluoroethanol) react smoothly with benzene at approximately room temperature in trifluoroethanol solvent to yield methane and the corresponding phenyl Pt(II) cations, via Pt(IV)-methyl-phenyl-hydrido intermediates. The reaction products of methyl-substituted benzenes suggest an inherent reactivity preference for aromatic over benzylic C–H bond activation, which can however be overridden by steric effects. For the reaction of benzene with cationic Pt(II) complexes bearing 3,5-disubstituted aryl diimine ligands, the rate-determining step is C–H bond activation, whereas for the more sterically crowded analogues with 2,6-dimethyl-substituted aryl groups, benzene coordination becomes rate-determining. This switch is manifested in distinctly different isotope scrambling and kinetic deuterium isotope effect patterns. The more electron-rich the ligand is, as assayed by the CO stretching frequency of the corresponding carbonyl cationic complex, the faster the rate of C–H bond activation. Although at first sight this trend appears to be at odds with the common description of this class of reaction as electrophilic, the fact that the same trend is observed for the two different series of complexes, which have different rate-determining steps, suggests that this finding does not reflect the actual C–H bond activation process, but rather reflects only the relative ease of benzene displacing a ligand to initiate the reaction; that is, the change in rates is mostly due to a ground-state effect. The stability of the aquo complex ground state in equilibrium with the solvento complex increases as the diimine ligand is made more electron-withdrawing. Several lines of evidence, including the mechanism of degenerate acetonitrile exchange for the methyl-acetonitrile Pt(II) cations in alcohol solvents, suggest that associative substitution pathways operate to get the hydrocarbon substrate into, and out of, the coordination sphere; that is, the mechanism of benzene substitution proceeds by a solvent (TFE)-assisted associative pathway.

Introduction

Extensive research over the last 30 years aimed at the selective functionalization of alkanes by transition metal complexes¹ has discovered many examples of inter- and intramolecular C–H bond activation. Relatively few examples, however, lead to actual alkane functionalization.² We have concentrated on an example of electrophilic activation of alkanes by late transition metal complexes,³ the so-called Shilov system (eq 1), in which

Pt(II) catalyzes oxidation of alkanes to alcohols by Pt(IV) at 120 °C.⁴ This system is not yet practical because it requires an expensive stoichiometric oxidant, the catalyst is unstable with respect to Pt metal formation, and rates are too slow, but it does exhibit patterns of regioselectivity ($1^\circ > 2^\circ \gg 3^\circ$)^{1d} as well as chemoselectivity (C–H bonds of RCH₃ are activated in preference to C–H bonds of RCH₂OH)⁵ that would be of considerable practical interest if the above problems could be solved.

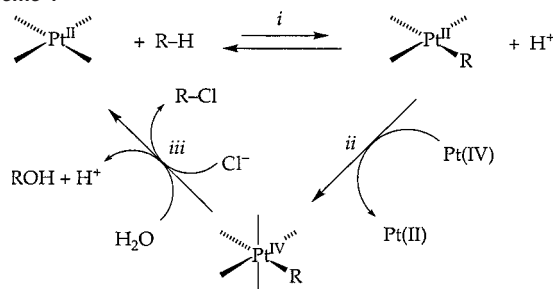


Studies by our group^{5,6} and others⁷ implicate a catalytic cycle consisting of three steps: (i) electrophilic activation of the alkane to yield a Pt(II)-alkyl compound; (ii) oxidation to a Pt(IV)-alkyl

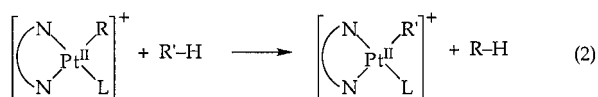
- (1) (a) Arndtsen, B. A.; Bergman, R. G.; Mobley, T. A.; Peterson, T. H. *Acc. Chem. Res.* **1995**, *28*, 154. (b) *Selective Hydrocarbon Activation*; Davies, J. A., Watson, P. L., Liebman, J. F., Greenberg, A., Eds.; VCH: New York, 1990. (c) *Activation and Functionalization of Alkanes*; Hill, C. L., Ed.; John Wiley & Sons: New York, 1989. (d) Shilov, A. E.; Shul'pin, G. B. *Activation and Catalytic Reactions of Saturated Hydrocarbons in the Presence of Metal Complexes*; Kluwer Academic Publishers: Dordrecht, 2000.
- (2) For some examples, see: (a) Periana, R. A.; Taube, D. J.; Gamble, S.; Taube, H.; Satoh, T.; Fujii, H. *Science* **1998**, *280*, 560–564. (b) Periana, R. A.; Taube, D. J.; Eviitt, E. R.; Löffler, D. G.; Wentreck, P. R.; Voss, G.; Masuda, T. *Science* **1993**, *259*, 340–343. (c) Waltz, K. M.; Hartwig, J. F. *J. Am. Chem. Soc.* **2000**, *122*, 11358–11369. (d) Chen, H. Y.; Schlecht, S.; Semple, T. C.; Hartwig, J. F. *Science* **2000**, *287*, 1995–1997. (e) Liu, F.; Pak, E. B.; Singh, B.; Jensen, C. M.; Goldman, A. S. *J. Am. Chem. Soc.* **1999**, *121*, 4086–4087. (f) Sen, A.; Benvenuto, M. A.; Lin, M.; Hutson, A. C.; Basicckes, N. *J. Am. Chem. Soc.* **1994**, *116*, 998–1003. (g) Jia, C.; Kitamura, T.; Fujiwara, Y. *Acc. Chem. Res.* **2001**, *34*, 633–639.

- (3) Stahl, S.; Labinger, J. A.; Bercaw, J. E. *Angew. Chem., Int. Ed.* **1998**, *37*, 2181–2192.
- (4) Gol'dshleger, N. F.; Es'kova, V. V.; Shilov, A. E.; Shteinman, A. A. *Zh. Fiz. Khim.* **1972**, *46*, 1353–1354 (English translation **1972**, *46*, 785–786).
- (5) Labinger, J. A.; Herring, A. M.; Lyon, D. K.; Luinstra, G. A.; Bercaw, J. E.; Horvath, I. T.; Eller, K. *Organometallics* **1993**, *12*, 895–905.

Scheme 1



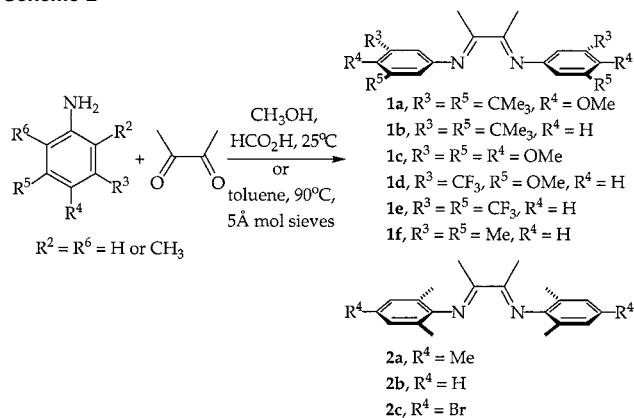
by $[\text{PtCl}_6]^{2-}$ via electron transfer; and (iii) nucleophilic attack by water or chloride ion at the alkyl to regenerate the Pt(II) complex and release the functionalized alkane (Scheme 1). Studies of protonolysis of R-Pt(II), the microscopic reverse of C–H activation, were carried out on model systems to shed some light on the nature of step (i) and led to the conclusion that two intermediates are involved: a Pt(II)-C,H- η^2 -alkane complex and a Pt(IV)-alkyl-hydrido complex.⁸ These studies further suggested that cationic complexes of the form $[(\text{N}-\text{N})\text{PtR}(\text{L})]^+$, where N–N is a bidentate diamine or diimine and L is a weakly bound solvent molecule or other ligand, should be capable of activating C–H bonds according to eq 2.



Two different examples confirming this prediction, where N–N is tetramethylethylenediamine and L is pentafluoropyridine,⁹ or N–N is $\text{Ar}^f\text{N}=\text{C}(\text{Me})-\text{C}(\text{Me})=\text{NAr}^f$ ($\text{Ar}^f = 3,5\text{-(CF}_3)_2\text{C}_6\text{H}_3$) and L is water and/or trifluoroethanol (TFE),¹⁰ were subsequently reported.

The complexes with N–N as an α -diimine ligand and L as H_2O /TFE are particularly well suited for mechanistic investigation, since many reactions take place at a convenient rate at or near room temperature, and since the steric and electronic properties of the ligands can easily be varied. A detailed kinetics and mechanistic study on the reaction of $[(\text{ArN}=\text{CMe}-\text{CMeN}=\text{Ar})\text{PtMe}(\text{L})]^+$ ($\text{Ar} = 2,6\text{-(CH}_3)_2\text{C}_6\text{H}_3$) with benzene supported the involvement of the two intermediates cited above, as well as a Pt(II)-(π -C,C- η^2 -benzene) complex, the formation of which appears to be the rate-determining step.¹¹ Yet several key questions remain unanswered. In particular, how does the reaction depend on the electronic and steric properties of the

Scheme 2



metal center? One might intuitively expect that for these formally electrophilic activations, a more electron-deficient metal center would lead to a faster reaction. However, it is not clear whether the term “electrophilic” has real mechanistic significance or merely describes stoichiometry. Indeed, a recent observation for a related reaction of a cationic Ir complex suggests the *opposite* trend: the more electron-rich center appears to react faster.¹² Changes in ligand properties might even change the rate-determining step, with possible consequences for selectivity. It is also unclear whether hydrocarbon enters the coordination sphere via an associative or dissociative mechanism.

To address some of these issues, we have initiated a series of kinetic and mechanistic investigations on the C–H activation of benzene by $[(\text{ArN}=\text{C}(\text{R})-\text{C}(\text{R})\text{N}=\text{Ar})\text{Pt}(\text{Me})(\text{L})]^+(\text{BF}_4)^-$ ($\text{R} = \text{Me}$ or H , $\text{L} = \text{H}_2\text{O}$ /TFE) in which both the steric and the electronic properties of Ar, and hence the overall complex, are varied over a significant range. We have also examined substitution reactions in the same system ($\text{L} = \text{MeCN}$). On the basis of these and other recent findings, we can construct a mechanistic description which appears consistent with all observations, even though it may fall somewhat short of a complete explanation.

Results

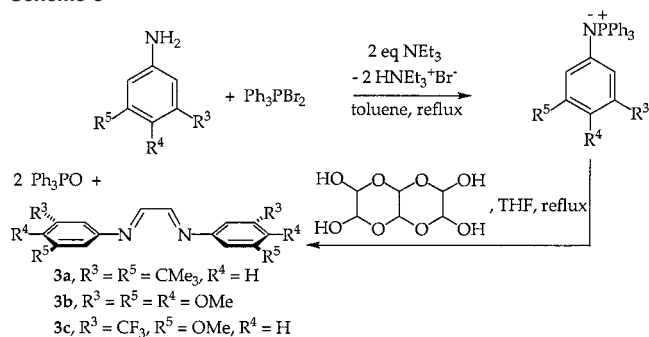
Synthesis of Diimine Ligands. The diimines $\text{ArN}=\text{CMe}-\text{CMeN}=\text{Ar}$ (**1**, $\text{Ar} = 3\text{-R}^3\text{-4-R}^4\text{-5-R}^5\text{-C}_6\text{H}_2$; **2**, $\text{Ar} = 2,6\text{-(CH}_3)_2\text{-4-R}^4\text{-C}_6\text{H}_2$), formally derivatives of 1,4-diazabutadiene, are prepared in moderate to good yields by condensing 2,3-butanedione and the corresponding anilines in methanol with a catalytic amount of formic acid or in toluene at 90 °C over 5 Å molecular sieves¹³ (Scheme 2). The latter procedure is particularly effective for the more electron-withdrawing anilines, and the use of 5 Å molecular sieves is crucial to obtain a reasonable yield of the products.

For comparison we wanted to have some examples of the analogous ligands *without* the backbone methyl substituents, $\text{ArN}=\text{CH}-\text{CHN}=\text{Ar}$. Although reactions between 3,5-disubstituted anilines and glyoxal¹⁴ invariably yielded mixtures,

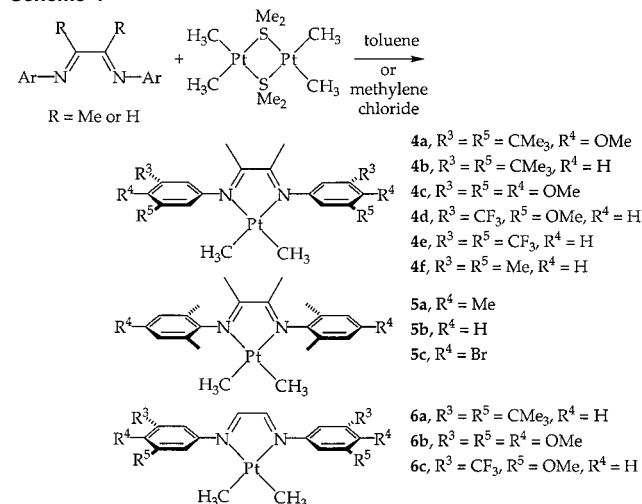
- (6) (a) Luinstra, G. A.; Wang, L.; Stahl, S. S.; Labinger, J. A.; Bercaw, J. E. *Organometallics* **1994**, *13*, 755–756. (b) Luinstra, G. A.; Labinger, J. A.; Bercaw, J. E. *J. Am. Chem. Soc.* **1993**, *115*, 3004–3005. (c) Luinstra, G. A.; Wang, L.; Stahl, S. S.; Labinger, J. A.; Bercaw, J. E. *J. Organomet. Chem.* **1995**, *504*, 75.
- (7) (a) Kushch, L. A.; Lavrushko, V. V.; Misharin, Y. S.; Moravskii, A. P.; Shilov, A. E. *Nouv. J. Chim.* **1983**, *7*, 729–733. (b) Hutson, A. C.; Lin, M.; Basicic, N.; Sen, A. *J. Organomet. Chem.* **1995**, *504*, 69–74. (c) Horvath, I. T.; Cook, R. A.; Millar, J. M.; Kiss, G. *Organometallics* **1993**, *12*, 8–10.
- (8) (a) Stahl, S. S.; Labinger, J. A.; Bercaw, J. E. *J. Am. Chem. Soc.* **1996**, *118*, 5961–5976. (b) Stahl, S. S.; Labinger, J. A.; Bercaw, J. E. *J. Am. Chem. Soc.* **1995**, *117*, 9371–9372.
- (9) (a) Holtcamp, M. W.; Henling, L. M.; Day, M. W.; Labinger, J. A.; Bercaw, J. E. *Inorg. Chim. Acta* **1998**, *270*, 467–478. (b) Holtcamp, M. W.; Labinger, J. A.; Bercaw, J. E. *J. Am. Chem. Soc.* **1997**, *119*, 848–849. (c) Holtcamp, M. W.; Labinger, J. A.; Bercaw, J. E. *Inorg. Chim. Acta* **1997**, *265*, 117–125.
- (10) Johansson, L.; Ryan, O. B.; Tilsel, M. *J. Am. Chem. Soc.* **1999**, *121*, 1974–1975.
- (11) Johansson, L.; Tilsel, M.; Labinger, J. A.; Bercaw, J. E. *J. Am. Chem. Soc.* **2000**, *122*, 10846–10855.

- (12) (a) Tellers, D. M.; Skoog, S. J.; Bergman, R. G.; Gunnoe, T. B.; Harman, W. D. *Organometallics* **2000**, *19*, 2428–2432. (b) Tellers, D. M.; Bergman, R. G. *J. Am. Chem. Soc.* **2000**, *122*, 954–955. (c) Tellers, D. M.; Yung, C. M.; Arndtsen, B. A.; Adamson, D. R.; Bergman, R. G. *J. Am. Chem. Soc.* **2002**, *124*, 1400–1410.
- (13) Westheimer, F. H.; Taguchi, K. *J. Org. Chem.* **1971**, *36*, 1570–1572.

Scheme 3



Scheme 4

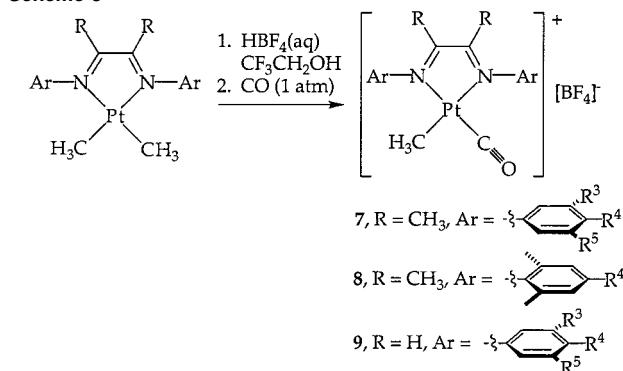


diimines **3** were prepared by reacting the corresponding iminophosphoranes¹⁵ with glyoxal trimer (Scheme 3).¹⁶

Preparation of Platinum Dimethyl Complexes. Diimine ligands **1–3** react with bis(dimethyl(μ -dimethyl sulfide)platinum(II))¹⁷ in toluene at room temperature to afford the corresponding platinum dimethyl complexes **4–6** in high yields (Scheme 4). The most useful feature for characterization is the [Pt–CH₃] signal, with its accompanying ¹⁹⁵Pt satellites, in the ¹H NMR. The shift is somewhat ligand-dependent, but the two-bond platinum coupling is virtually the same, ~85 Hz, for all these dimethyl complexes.

Preparation of Platinum(II) Methyl Carbonyl Cations. Addition of 1 equiv of HBF₄ (aq) to a solution of **4–6** in trifluoroethanol generates a mixture of solvento and aquo adducts (vide infra) of the platinum(II) methyl cation, which upon exposure to 1 atm of carbon monoxide converts cleanly to the corresponding platinum methyl carbonyl cation **7–9** (Scheme 5).

Scheme 5



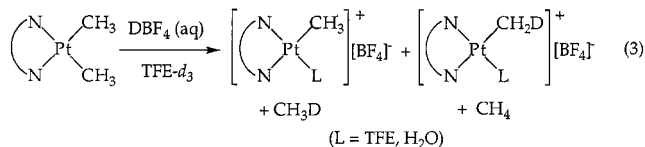
In many instances, addition of CO causes the solution to change from orange or red to yellow almost instantaneously (except for **9b**, in which case the solution turned to wine red). The Pt–CH₃ resonances (in CD₂Cl₂) shift ~0.2 ppm upfield as compared to those of the corresponding dimethyl complexes, while ²J_{Pt–H} decreases from ~85 to ~66 Hz. As a result of the reduced symmetry, the backbone R groups are now inequivalent, which is displayed in the NMR spectra, particularly in the ³J_{Pt–H} values.

All the carbonyl cations appear to be indefinitely stable in trifluoroethanol under 1 atm of CO, but **7d** and **7e** decompose rapidly in the solid state or in methylene chloride in the absence of excess CO. In TFE-*d*₃, the backbone methyls of **7e** became fully deuterated within an hour at room temperature. Isolated **9b** appeared to contain a small amount of paramagnetic material that significantly broadened the spectrum. The carbonyl IR stretching frequencies of complexes **7–9** are reported in Table 1.

Generation of Platinum(II) Methyl-Aquo/Solvento Cations. Protonolysis of Pt(II) dimethyl complexes **4–6** by aqueous HBF₄ in TFE generates the corresponding methyl cations as an equilibrium mixture of aquo and solvento adducts **10–12** (Scheme 6).^{10,11}

The stoichiometry need not be exactly 1:1, as the Pt–Me groups of cationic complexes do not readily react with the slight excess of acid. Subsequent addition of a slight excess of acetonitrile (or carrying out the initial protonolysis in acetonitrile solution) affords the acetonitrile adducts **13–15**. The platinum satellites for the Pt–CH₃ signals for **10–12** are extremely broad, in contrast to the relatively sharp satellites observed for the corresponding carbonyl (**7–9**) and acetonitrile (**13–15**) adducts.

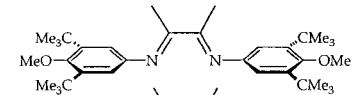
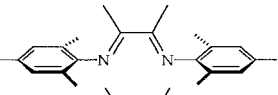
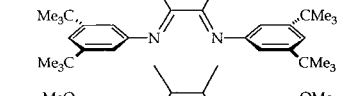
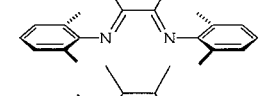
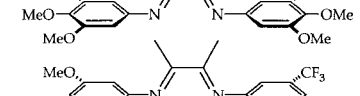
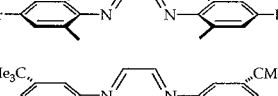
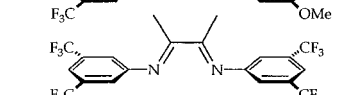
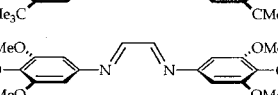
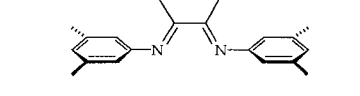
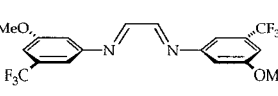

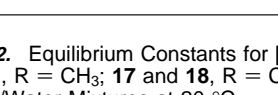
Protonolysis of **4–6** in TFE-*d*₃ results in liberation of CH₄ as well as CH₃D, with concomitant formation of [Pt–CH₂D] and [Pt–CH₃] cations (eq 3).

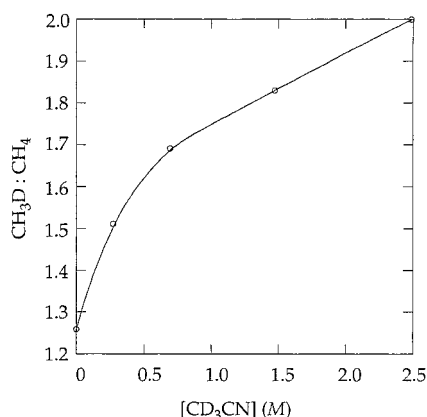
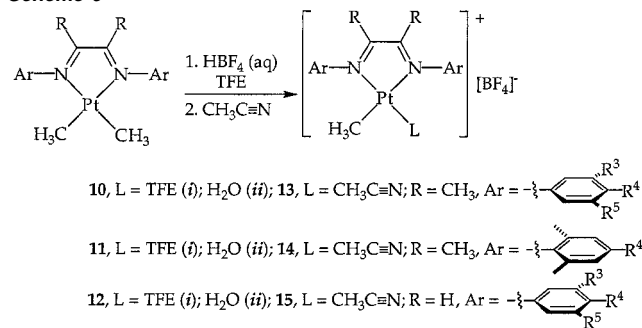


Within integration error limits, the ratio of CH₄ to CH₃D equals that of [Pt–CH₂D] to [Pt–CH₃]. No multiple deuteration was observed for either the methane or the [Pt–methyl]. When protonolysis of **4b** was carried out in the presence of added acetonitrile, the ratio of CH₃D to CH₄ was found to increase with the acetonitrile concentration (Figure 1).

- (14) Kliegman, J. M.; Barnes, R. K. *J. Org. Chem.* **1970**, *35*, 3140–3143. 2,6-Dimethylaniline and its derivatives do react fairly cleanly with glyoxal (40% aqueous) to yield the corresponding diimines.
- (15) (a) Saito, T.; Ohkubo, T.; Kuboki, H.; Maeda, M.; Tsuda, K.; Karakasa, T.; Satsumabayashi, S. *J. Chem. Soc., Perkin Trans. 1* **1998**, 3065–3080. (b) Nitta, M.; Soeda, H.; Iino, Y. *Bull. Chem. Soc. Jpn.* **1990**, *63*, 932–934. (c) Hartmann, R. W.; Vom Orde, H. D.; Heindl, A.; Schoenenberger, H. *Arch. Pharm. (Weinheim, Ger.)* **1988**, *321*, 497–501. (d) Soloshonok, V. A.; Gerus, I. I.; Yagupol'skii, Y. L.; Kukhar, V. P. *Zh. Org. Khim.* **1987**, *23*, 2308–2313.
- (16) Iminophosphoranes containing extremely electron-withdrawing substituents (e.g., Ar = 3,5-(CF₃)₂-C₆H₃) do not react with glyoxal trimer in refluxing THF. The corresponding diimines can only be prepared by reacting the iminophosphoranes with glyoxal monomer at room temperature in methylene chloride. For preparation of glyoxal monomer, see: Wang, Y.; Arif, A. M.; Gladysz, J. A. *Organometallics* **1994**, *13*, 2164–2169.
- (17) Hill, G. S.; Irwin, M. J.; Levy, C. J.; Rendina, L. M.; Puddephatt, R. J. *Inorg. Synth.* **1998**, *32*, 149–153.

Table 1. Infrared Carbonyl Stretching Frequencies for [(N–N)Pt(CH₃)(CO)]⁺[BF₄][–] (**7**–**9**) in Methylene Chloride Solution

N–N		ν_{CO} (cm ^{–1})	N–N		ν_{CO} (cm ^{–1})
7a		2103.5(3)	8a		2108.3(3)
7b		2104.6(3)	8b		2109.6(3)
7c		2105.8(3)	8c		2111.1(3)
7d		2110.1(3)	9a		2108.8(3)
7e		2113.5(3)	9b		2110.3(3)
7f		2105.7(3)	9c		2116.0(3)

**Figure 1.** The ratio of CH₃D:CH₄ generated in the protonolysis of **4b** in TFE-*d*₃ as a function of acetonitrile concentration.**Scheme 6**

Cations **10**–**12** decompose over the course of several weeks at room temperature in TFE solution. For **10a/b** and **12a**, a single (or major) species is formed, accompanied by methane liberation. NMR (¹H and ¹⁹F) is consistent with a (μ -OH)₂ dimeric structure (**16**). This was confirmed for **16b**, the decomposition product of **10b**, by a crystal structure determination.¹⁸ The analogous phenyl complexes **17** and **19** (vide infra) react similarly, evolving benzene (eq 4). In contrast, the decomposition of **11** yielded a mixture of unidentifiable products. The

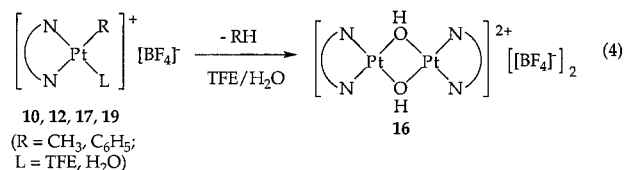
(18) Rostovtsev, V. V.; Labinger, J. A.; Bercaw, J. E., unpublished results.

Table 2. Equilibrium Constants for [(N–N)Pt(R)(L)]⁺[BF₄][–] (**10** and **11**, R = CH₃; **17** and **18**, R = C₆H₅; *i*, L = TFE; *ii*, L = H₂O) in TFE/Water Mixtures at 20 °C

	$10i \rightleftharpoons 10ii$	$17i \rightleftharpoons 17ii$
a (R ³ = R ⁵ = CMe ₃ , R ⁴ = OMe)	3.9×10^2	6.6×10^2
b (R ³ = R ⁵ = CMe ₃ , R ⁴ = H)	4.3×10^2	7.4×10^2
c (R ³ = R ⁴ = R ⁵ = OMe)	7.5×10^2	9.6×10^2
d (R ³ = OMe, R ⁵ = CF ₃ , R ⁴ = H)	1.4×10^3	1.8×10^3
e (R ³ = R ⁵ = CF ₃ , R ⁴ = H)	2.8×10^3	4.0×10^3

	$11i \rightleftharpoons 11ii$	$18i \rightleftharpoons 18ii$
a (R ² = R ⁶ = Me, R ⁴ = Me)	7.8×10^2	1.5×10^3
b (R ² = R ⁶ = Me, R ⁴ = H)	9.5×10^2	1.8×10^3
c (R ² = R ⁶ = Me, R ⁴ = Br)	1.6×10^3	3.1×10^3

decomposition is accelerated by higher platinum concentrations and retarded by added water; the mechanism for the formation of the (μ -OH)₂ dimer is not clear.



Equilibria between Aquo and Solvento Complexes. Addition of 1 equiv of aqueous HBF₄ (which contains approximately 5 mol of H₂O per mole of HBF₄) at 20 °C to a suspension of 0.007 mmol of (**4**) in 0.7 mL of TFE-*d*₃ results in two Pt–CH₃ signals in the ¹H NMR, in ratios ranging from ~1.5:1 (**10a**) to >10:1 (**10e**). For **10a**, addition of water further increases the relative intensity of the major peak, which is accordingly assigned to aquo complex **10a_{ii}**. The equilibrium between the solvento and aquo adducts (eq 5) greatly favors the latter for all ligands examined here. The magnitude of the equilibrium constant depends on the ligands (Table 2): the more electron-withdrawing the diimine substituents (indicated by a higher carbonyl stretching frequency for the analogous methylcarbonyl cation, vide supra), the larger the equilibrium constant. Moreover, for the same diimine ligand, the equilibrium constant for the platinum(II) phenyl cation (**17** and **18**) is greater than

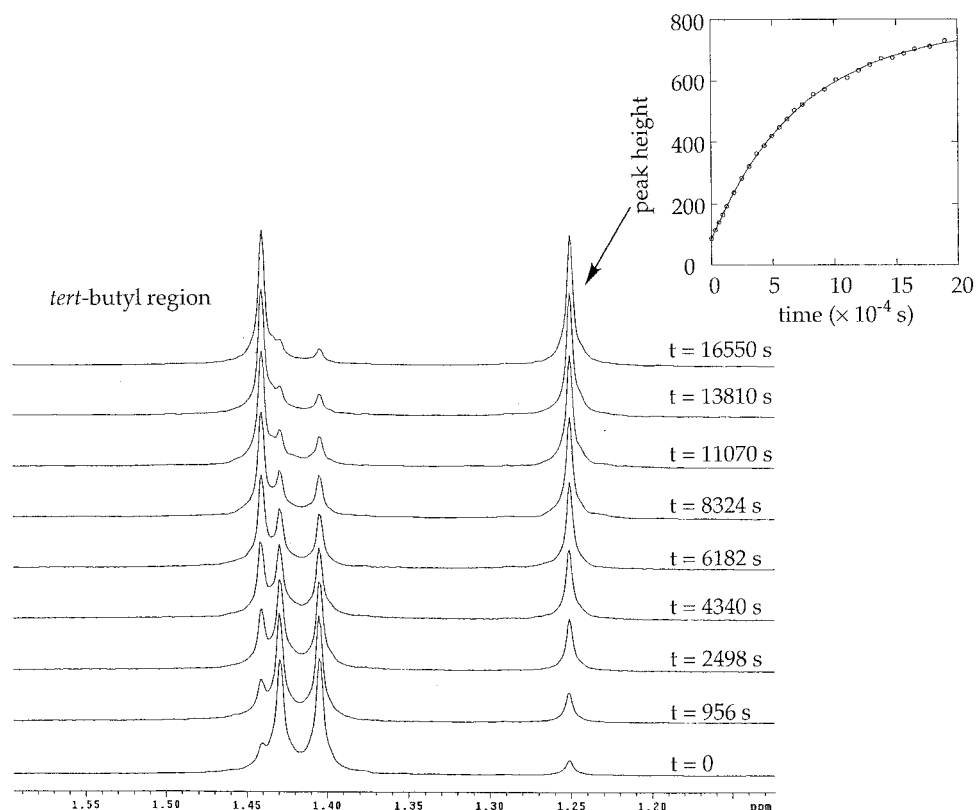
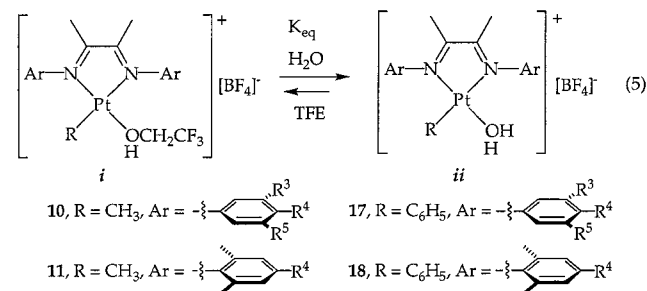


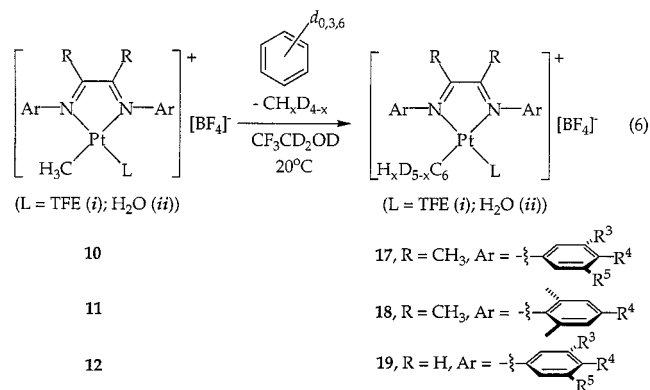
Figure 2. The *tert*-butyl region of the ^1H NMR spectra, showing changes for the reaction between benzene and **10b** ($[\text{D}_2\text{O}] = 2.72 \text{ M}$, $[\text{C}_6\text{H}_6] = 0.49 \text{ M}$, $[\text{Pt}] = 0.01 \text{ M}$). The inset shows an exponential curve fit of the peak height at 1.25 ppm vs time.

for the methyl cation (**10** and **11**). The equilibrium constants for **12** and **19** are too large to be determined accurately; they are all greater than 3×10^3 .



Reactions between Platinum(II) Methyl Cations and Benzene. Platinum(II) methyl cations **10–12** react cleanly with benzene, or with partially or completely deuterated benzene (*vide infra*), to form the corresponding platinum(II) phenyl complexes **17–19** respectively, with concurrent production of methane (eq 6).

Under reaction conditions where both the solvent and the aquo cations are observable by ^1H NMR, the two species disappear at the same rate, and the solvent and aquo adducts of the phenyl products appear at the same rate. No other species were observed up to 3 half-lives; the $(\mu\text{-OH})_2$ dimers **16** can be observed at later stages of the reaction. In all cases the rates of $(\mu\text{-OH})_2$ dimer formation (eq 4) from either the starting materials **10–12** or the products **17–19** are at least an order of magnitude slower than those of benzene C–H bond activation, so the rate constants reported below should not be affected by this secondary reaction to any significant degree.



Kinetics of Benzene C–H Bond Activation. ^1H NMR was used to monitor the disappearance of starting material and/or the appearance of product, from which rates were determined. Figure 2 shows the results of a typical experiment, for the reaction between **10b** ($[\text{D}_2\text{O}] = 2.72 \text{ M}$, where only aquo adducts are detectable) and benzene in TFE-*d*₃. The values of the calculated rate constants, k_{obs} , for the various complexes under different sets of conditions can be found in the Supporting Information (Tables S1–S12). Additional kinetics experiments were carried out in several cases, particularly for **10a** and **10b**. The reaction rates are not affected by ionic strength; for example, the observed rate constant for the reaction between **10a** and benzene at $[\text{D}_2\text{O}] = 1.33 \text{ M}$, $[\text{C}_6\text{H}_6] = 0.25 \text{ M}$, and $[\text{Pt}] = 0.01 \text{ M}$ is $(1.8 \pm 0.2) \times 10^{-4} \text{ s}^{-1}$ with no added NMe_4BF_4 and $(1.9 \pm 0.2) \times 10^{-4} \text{ s}^{-1}$ with $[\text{NMe}_4\text{BF}_4] = 0.12 \text{ M}$. Hence most of the kinetic studies were run without controlling ionic strength. However, it should be noted that the rates did show a slight

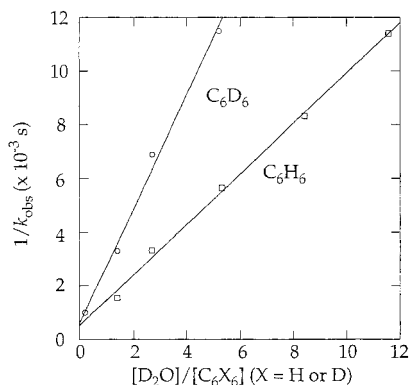


Figure 3. The inverse of observed rate constants in the reactions of **10a** with benzene varies linearly with the water:benzene concentration ratio.

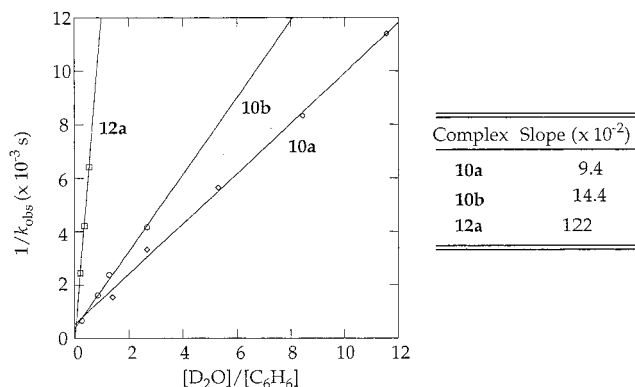


Figure 4. For the reactions of various Pt(II) methyl cations with benzene, the inverse of observed rate constants is linear with respect to the water:benzene concentration ratio. The slopes of the lines vary greatly from cation to cation.

decrease in the presence of weakly coordinating anions such as triflate (Table S12).

As previously found for **11b**,¹¹ the rates of benzene C–H bond activation are decreased by added water, and $1/k_{\text{obs}}$ is linear with respect to $[\text{D}_2\text{O}]/[\text{C}_6\text{H}_6]$ (Figure 3). The slope of the line (and, thus, k_{obs}) depends significantly on the ligand (Figure 4). The plot of k_{obs} versus $[\text{C}_6\text{H}_6]/[\text{D}_2\text{O}]$ deviates from linearity at very low water concentrations (Figure 5).

The temperature dependence was studied over the range of 0–55 °C for the reaction between **10b** and C_6H_6 and over the range of 0–30 °C for the reaction between **10b** and C_6D_6 . The water concentration was kept sufficiently high such that aquo adducts account for >90% of the Pt(II) species. The overall activation parameters were calculated from Eyring plots, such as the one shown in Figure 6, and give $\Delta H^\ddagger = 20 \text{ kcal mol}^{-1}$, $\Delta S^\ddagger = 5 \text{ e.u.}$ for C_6H_6 activation and $\Delta H^\ddagger = 20.5 \text{ kcal mol}^{-1}$, $\Delta S^\ddagger = 6 \text{ e.u.}$ for C_6D_6 activation. The entropy of activation may be contrasted to that found for **11b**, for which a ΔS^\ddagger of -16 e.u. was measured.¹¹

Deuterium Scrambling. Earlier studies on **11b**¹¹ found that (a) <5% deuterium incorporation was observed in the methane generated in the reactions with C_6H_6 in TFE- d_3 and (b) nearly complete statistical scrambling of isotopes takes place in the reaction with either C_6D_6 or 1,3,5- $\text{C}_6\text{H}_3\text{D}_3$. For complexes **10**, again, there is no incorporation of label from solvent, but in contrast there is only partial scrambling of protium and deuterium among the methyl group and deuteriobenzenes. For example, when **10b** reacts with C_6D_6 , the methane evolved

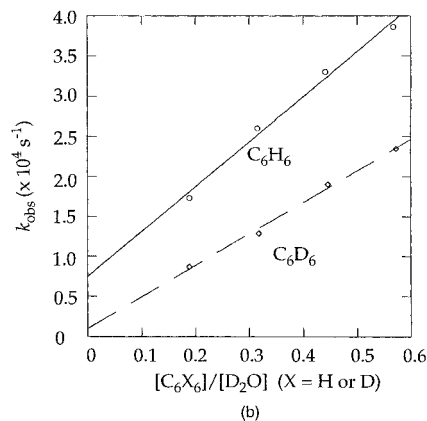
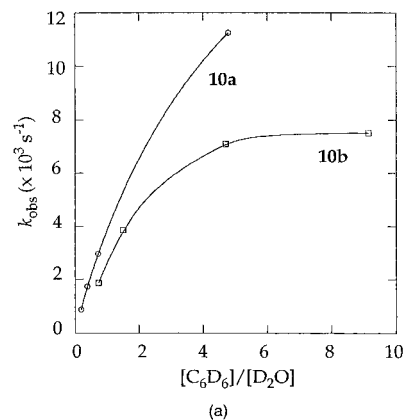


Figure 5. (a) A plot of k_{obs} vs $[\text{C}_6\text{D}_6]/[\text{D}_2\text{O}]$ deviates from linearity at low water concentrations ($[\text{Pt}] = 0.01 \text{ M}$, $[\text{C}_6\text{D}_6] = 0.25 \text{ M}$). (b) For reactions of **10a** and benzene at high water concentrations, k_{obs} is linear with respect to $[\text{C}_6\text{D}_6]/[\text{D}_2\text{O}]$ ($[\text{Pt}] = 0.01 \text{ M}$, $[\text{D}_2\text{O}] = 1.23\text{--}1.30 \text{ M}$).

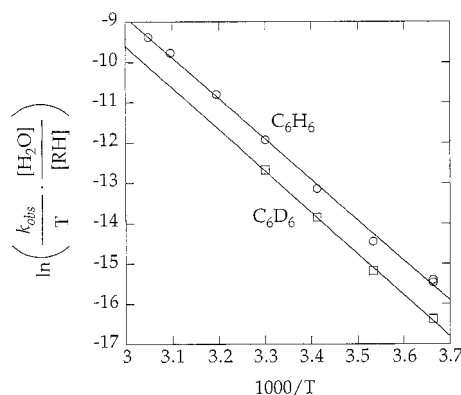


Figure 6. Eyring plot for the reactions of **10b** with C_6H_6 and C_6D_6 .

consists mostly of CH_3D (~60%) and CH_2D_2 (~30%). Even less scrambling is observed for complexes **12**. For example, when **12a** reacts with C_6D_6 , CH_2D_2 and higher isotopomers account for <10% of the liberated methane. ^1H NMR shows that label is also incorporated into the methyl group of unreacted starting material, up to ~20% of $[\text{Pt}\text{--}\text{CH}_2\text{D}]$. For **11a** and **11c** the results are very similar to those of **11b**: reactions with C_6D_6 produce CH_2D_2 and CHD_3 as the major methane isotopomers, although deuterium incorporation into the unreacted platinum-methyl group is observed here as well.

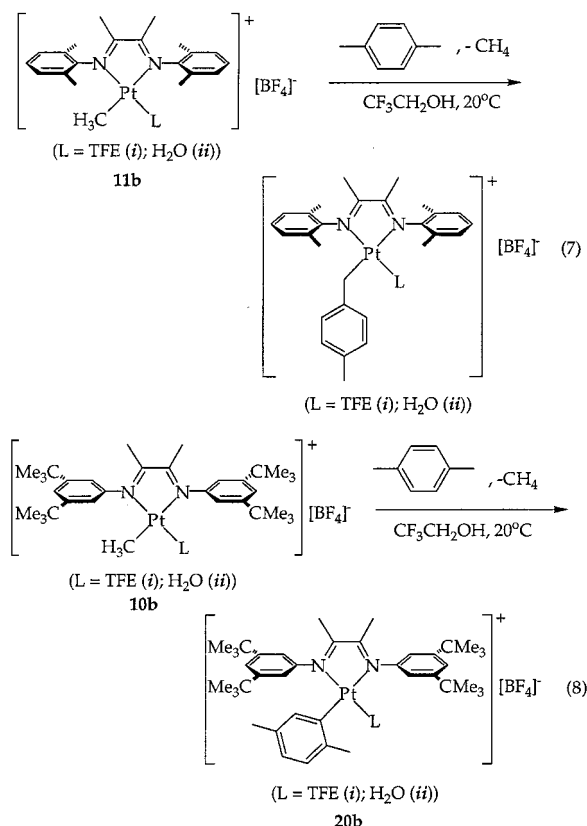
Kinetic Deuterium Isotope Effects (KIEs). KIEs were determined by three different methods: (1) in parallel reactions, separately determining the rate constants for reactions of C_6H_6 and C_6D_6 under the same conditions; (2) intermolecular

Table 3. Kinetic Deuterium Isotope Effects for Benzene C–L (L = H, D) Bond Activation Reactions

complex	T (°C)	method	k _H /k _D	complex	T (°C)	method	k _H /k _D
10a	20	parallel	2.0	10e	20	parallel	2.2
10b	20	parallel	2.2	11a	35	parallel	1.1
10b	20	1,3,5-C ₆ H ₃ D ₃	1.8	11b	35	parallel	1.1
10b	20	1:1 C ₆ H ₆ :C ₆ D ₆	1.9	11c	35	parallel	1.1
10c	20	parallel	1.9	12a	20	parallel	5.0
10c	20	1:1 C ₆ H ₆ :C ₆ D ₆	1.6	12b	20	parallel	3.6
10d	20	parallel	2.2	12c	20	parallel	5.9
10d	20	1:1 C ₆ H ₆ :C ₆ D ₆	2.0				

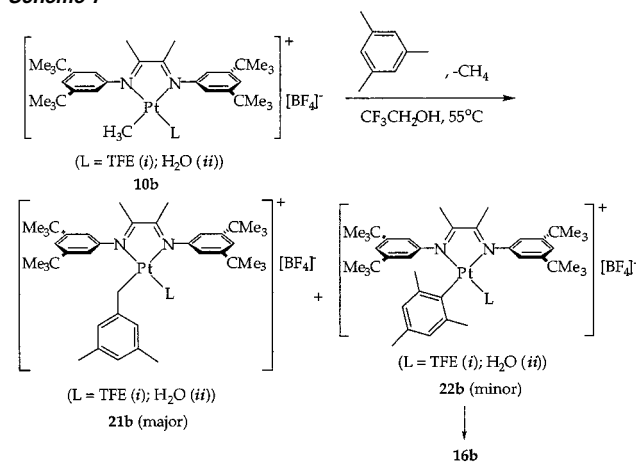
competition, determining (by ¹H NMR) the isotopic composition of methane liberated in reaction with 1:1 C₆H₆:C₆D₆, and (3) intramolecular competition, using 1,3,5-C₆H₃D₃. The results are shown in Table 3. Note that the two competition methods give values that are consistently lower than those measured by parallel reactions (vide infra), although the differences are comparable to the uncertainties.¹⁹

Reactions of 10b with Other Aromatic Hydrocarbons. The regioselectivity for the C–H bond activation for alkyl-substituted aromatic compounds appears to be affected by the steric bulk of both the substrates and the ligand. Whereas **11b** reacts with *p*-xylene predominantly at the benzylic position (eq 7),²⁰ the reaction between **10b** and *p*-xylene results almost exclusively in aryl C–H bond activation (eq 8).



In contrast, the reaction between mesitylene and **10b** proceeds mainly through benzylic C–H bond activation (Scheme 7).

In the latter case, the selectivity for benzylic activation decreases at higher temperatures. At 25 °C, a ratio of 95:5 of

Scheme 7

benzylic activation product **21b** to aromatic activation product **22b** is observed, whereas at 55 °C, the selectivity drops to 3:1. The product resulting from aromatic C–H bond activation appears to be much less stable than that from benzylic C–H activation: during the reaction between **10b** and mesitylene, the ¹H NMR resonances corresponding to **22b** initially grow in intensity and then disappear gradually, with formation of (μ-OH)₂ dimer **16b**. Compared to benzene C–H bond activation, the reaction between **10b** and *p*-xylene is approximately 3 times slower, while that with mesitylene is approximately 10 times slower.

The kinetic deuterium isotope effects for reactions between **10b** and *p*-xylene and mesitylene were measured (parallel reactions method at 25 °C). These also appear to depend on steric bulk of the substrates: *k*_H/*k*_D = 2.2 for benzene (C₆X₆), 1.5 for *p*-xylene (C₆X₃(CX₃)₂), and 1.2 for mesitylene (C₆X₃(CX₃)₃) (X = H, D).

Electron-deficient or extremely bulky aromatic compounds react sluggishly, or not at all, with **10b** at room temperature. For example, when 30 equiv of 1,4-di(*tert*-butyl)benzene was added to a 0.01 M TFE-*d*₃ solution of **10b** ([D₂O] = 0.05 M), 85% of the starting material remained after 24 h at room temperature. The ¹H NMR of the reaction mixture showed several broad, as yet unidentified new peaks. Similarly, **10b** showed little reactivity toward pentafluorotoluene or 1,4-(CF₃)₂C₆H₄ after several hours at room temperature.

Acetonitrile Exchange Reactions. To shed some light on whether dissociative or associative substitution pathways operate in these systems, we briefly investigated the isotopic exchange between a Pt(II)-bound CH₃CN and free CD₃CN in several alcoholic solvents (Scheme 8), using ¹H NMR spectroscopy to follow the disappearance of bound acetonitrile and the appearance of free CH₃CN.

The rate constants for the exchange of **13b** in CD₃OD, as a function of CD₃CN concentration and temperature, are shown

(19) The estimated uncertainties are ~10–20% for the parallel reactions and 5–10% for the inter- and intramolecular competition reactions.

(20) Johansson, L.; Ryan, O. B.; Rømming, C.; Tilset, M. *J. Am. Chem. Soc.* **2001**, *123*, 6579–6590.

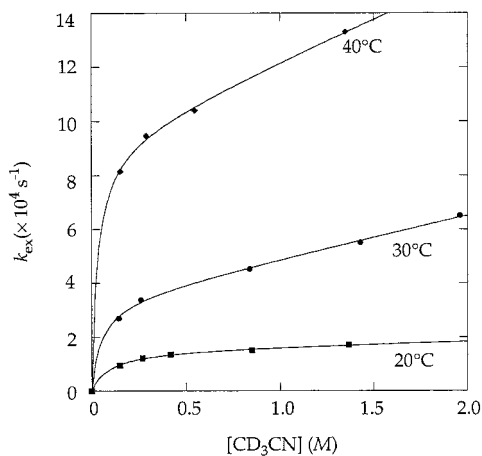


Figure 7. Plot of observed rate constants for exchange of free and bound acetonitrile vs free [acetonitrile] for **13b** at various temperatures.

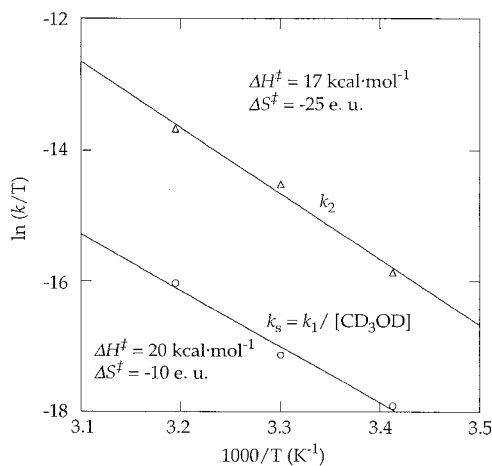
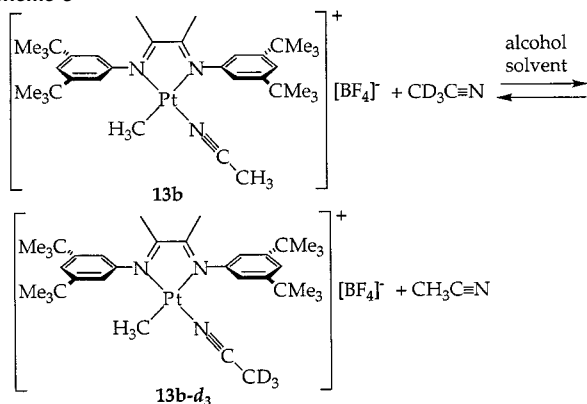


Figure 8. Eyring plots for second-order acetonitrile exchange rate constants for both the solvent-assisted pathway (k_s) and the direct-exchange pathway (k_2) for **13b**.

Scheme 8



in Figure 7. The shapes of the curves indicate a rate law of the form $k_{\text{ex}} = k_1 + k_2[\text{CD}_3\text{CN}]$, where the first term represents a dissociative or solvent-assisted pathway whose rate constant is determined from the intercept of the extrapolated linear part of the plot, and the second term represents a direct associative path whose rate is obtained from the slope of the latter. Eyring plots between 20 and 40 °C have been constructed for k_s ($= k_1/[\text{CD}_3\text{OD}]$) and k_2 (Figure 8); both lead to calculated negative entropies of activation, although the precision of the data and

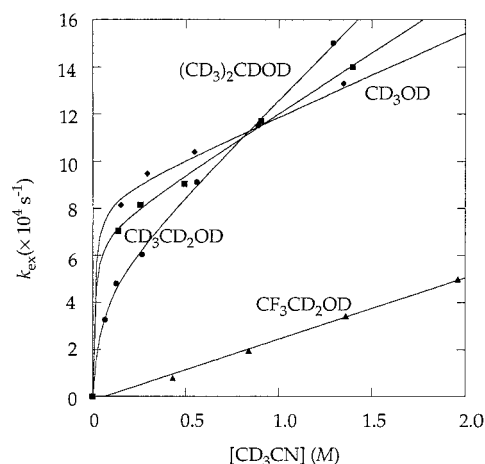


Figure 9. A plot of observed rate constants vs free acetonitrile concentrations for the isotopic exchange of bound (**13b**) and free acetonitrile in different solvents at 40 °C.

Table 4. Second-Order Rate Constants for the Acetonitrile Exchange Reactions for **13b** in Various Alcohol Solvents at 40 °C

solvent	$10^4 \times k_1$ (s^{-1})	$10^4 \times k_s$ ($\text{M}^{-1} \text{s}^{-1}$)	$10^4 \times k_2$ ($\text{M}^{-1} \text{s}^{-1}$)
methanol	8.4 ± 0.3	0.34 ± 0.01	3.6 ± 0.1
ethanol	6.7 ± 0.4	0.39 ± 0.02	5.2 ± 0.2
2-propanol	4.0 ± 0.3	0.31 ± 0.01	8.6 ± 0.2
TFE	<0.01	<0.01	2.6 ± 0.1

Table 5. Second-Order Rate Constants for the Acetonitrile Exchange Reactions of Various Pt(II) Methyl Cations in Methanol (30 °C) and TFE (40 °C)

complex	solvent	T (°C)	$10^4 \times k_1$ (s^{-1})	$10^4 \times k_s$ ($\text{M}^{-1} \text{s}^{-1}$)	$10^4 \times k_2$ ($\text{M}^{-1} \text{s}^{-1}$)
13b	methanol	30	2.7 ± 0.3	0.11 ± 0.01	1.5 ± 0.1
13d	methanol	30	9.9 ± 0.4	0.4 ± 0.02	7.9 ± 0.3
14b	methanol	30	2.6 ± 0.2	0.11 ± 0.01	1.8 ± 0.2
14c	methanol	30	6.3 ± 0.3	0.26 ± 0.02	4.4 ± 0.3
13b	TFE	40	<0.1	<0.1	2.6 ± 0.1
13d	TFE	40	— ^a	— ^a	— ^a
14b	TFE	40	<0.01	<0.01	2.8 ± 0.1
14c	TFE	40	<0.01	<0.01	10.2 ± 0.1

^a Acetonitrile exchange is too fast ($k_{\text{ex}} > 50 \times 10^{-4} \text{ s}^{-1}$) to measure rates.

the small range of temperatures limit our confidence in these values.

The exchange reactions in different solvents at 40 °C were also investigated, with the results shown in Figure 9. Rate constants were calculated in the same manner and are displayed in Table 4. We also briefly examined the dependence of the exchange rates on the ligands. Under similar conditions ($[\text{CD}_3\text{CN}] = 1.3 \text{ M}$, $T = 40 \text{ °C}$, solvent = TFE- d_3), the exchange between bound and free acetonitrile for **13d** (Ar = 3-OMe-5-CF₃-C₆H₃) is ca. 6–7 times faster than that for **13b** (Ar = 3,5-(CMe₃)₂-C₆H₃) and that for **14c** (Ar = 2,6-Me₂-4-Br-C₆H₂) is ca. 3.5 times faster than that for **14b** (Ar = 2,6-Me₂-C₆H₃). In contrast, the rates of exchange are approximately the same for **13b** and **14b** (Table 5).

In deuterated alcohols other than TFE- d_3 , competing deuteration of the backbone methyl groups is observed. The rate of deuteration not only depends on solvent and ligand, but is also regioselective; the deuteration of the two nonequivalent backbone methyl groups occurs at different rates in each case, with the higher field NMR signal exhibiting more rapid deuteration. For example, for **13b** in CD₃OD at 30 °C, <5%

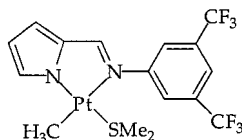
deuteration occurred after 1.5 h; whereas for **13d**, the higher field backbone methyl resonance was completely deuterated within 15 min, while <5% deuteration was observed for the low field one. For **13b** at 40 °C, <10% deuteration occurred after 1 h in CD₃OD, but in (CD₃)₂CDOD, the high field resonance was more than 80% deuterated after 15 min, and the low field resonance was ~40% deuterated after 1 h. Deuterium exchange is even faster for carbonyl cations; in **7e**, backbone deuteration occurred even in TFE-*d*₃ at room temperature, whereas no observable deuteration occurred for **7a–d** under these conditions.

Discussion

Synthesis and Characterization of Platinum Complexes.

The procedures for ligand synthesis, formation of dimethylplatinum complexes, and protonolysis to monomethylplatinum cations all appear to be quite general for a wide array of substituted diaryldiimine ligands, thus making systematic examination of the effects of ligand electronic and steric properties possible. The only exception is in the synthesis of **6c**, where it appeared necessary to periodically purge and remove free SMe₂, which can compete with the diimine ligand **3c** for the coordination to the Pt(II) center. It is particularly convenient that cationic Pt(II)-methyl complexes are not readily protonolyzed,^{9c} which permits their clean generation without requiring rigorous control of stoichiometry in adding an equivalent of acid.

All complexes prepared are characterized straightforwardly by ¹H NMR. The only important structural variable is the orientation of the aryl rings with respect to the coordination plane. Structural characterizations by Ruffo and co-workers on cationic Pt-methyl-olefin complexes with Ar = 2,6-diethylphenyl revealed a near-orthogonal orientation between the aryl rings and the Pt coordination plane.²¹ NMR studies by the same authors suggest there is hindered rotation around the N–C^{ipso} bond as well.²² Similar conclusions have also been reached by Eisenberg and co-workers, where they were readily able to isolate the meso and rac isomers of a neutral (diimine)PtMe₂ complex with Ar = 2-OMe-4,6-(*t*-Bu)₂-C₆H₂.²³ In comparison, few X-ray structures have been obtained for complexes containing diimine ligands with 3,5-disubstituted aryl substituents. Recently the crystal structure of a related pyrrolyl-imine complex (**23**) found the phenyl ring at 58° to the N–Pt–N plane.²⁴



23

The latter finding is consistent with AM1 level calculations on **4e**, which predict that the phenyl rings are ca. 60° tilted out of the N–Pt–N plane.²⁵ On the other hand, the X-ray structure of **16b** (R³ = R⁵ = CMe₃, R⁴ = H) showed the phenyl rings

are ca. 80° to the N–Pt–N planes.¹⁸ However, the bimetallic structure of **16b** with relatively short Pt–O bridges could cause the phenyl rings to rotate further out of the plane to avoid steric congestion. ¹H NMR signals of the complexes with 3,5-disubstituted aryldiimines are also consistent with rapid rotation around N–C^{ipso} bonds. For example, only one set of ligand and [Pt–CH₃] NMR peaks is observed for **4d** (which has asymmetrically substituted aryl groups) down to –40 °C, implying rotation about the C–N bond is fast on the NMR time scale. We expect this is the case for all 3,5-disubstituted aryls.

The ¹⁹⁵Pt satellites are useful NMR features, not only in facilitating assignments but also as qualitative probes of electronic effect transmission. In particular, for the methyl carbonyl cations the downfield signals for the backbone methyls (**7** and **8**) exhibit larger ⁴J_{Pt–H} values than the upfield signals. We tentatively assign the downfield resonances to the methyl adjacent to the N trans to CO; the large trans influence of methyl bonded to platinum would be expected to elongate the opposite Pt–N bond and reduce the corresponding coupling constant. Similarly, for **9**, the upfield signals for the backbone H exhibit ³J_{Pt–H} values (~74 Hz) nearly twice as large as those for the downfield ones (~38 Hz) and are consequently assigned to the H adjacent to the N trans to CO. Such effects have chemical as well as spectroscopic consequences, as manifested by the differential rates of deuteration of backbone methyls for complexes **13** in deuterated alcohols. We will not consider these effects in any detail here, except to note that they are consistent with the substantial perturbations of C–H bond activation by variation of diimine ligand electronic character, to be discussed below.

CO Stretching Frequencies as a Measure of Electronic Character. To examine electronic effects on C–H bond activation, we sought an empirical measure of actual electronic density at cationic Pt(II) as preferable to a semiempirical prediction of expected ligand properties. As ν_{CO} is a well-established probe of electron density at a metal center, we prepared the platinum methyl carbonyl cations with the various diimine ligands. These bands are quite sharp for solution samples, and the ν_{CO} values are shown in Table 1 and plotted against the Hammett substituent constants (σ = σ_p + σ_m)²⁶ in Figure 10. All three series, **7a–f**, **8a–c**, and **9a–c**, give fairly good linear correlations; however, the lines are well displaced from one another. In other words, for the same aryl σ values, the cations **8** show a higher CO stretching frequency, and thus are comparatively electron-poor, relative to **7**. For example, ν_{CO} for **7f** (Ar = 3,5-Me₂C₆H₃) is 2105.7(3) cm⁻¹ versus 2109.6(3) cm⁻¹ for **8b** (Ar = 2,6-Me₂C₆H₃), though one might expect that they should be reasonably electronically similar (both having dimethylaryl groups) and exhibit similar CO stretching frequencies. Why do they not?

Of course, as defined above the σ values for complexes **8** do not take account of the ortho methyl groups, as ortho substituent constants are considered unreliable owing to steric complications. Yet this cannot be the explanation, as σ for methyl is negative (electron-releasing relative to hydrogen); hence including a contribution for the ortho substituents would move the correlation line for **8** to the left, further from that for **7**. We

- (21) (a) Ganis, P.; Orabona, I.; Ruffo, F.; Vitagliano, A. *Organometallics* **1998**, *17*, 2646–2650. (b) Fusto, M.; Giordano, F.; Orabona, I.; Ruffo, F. *Organometallics* **1997**, *16*, 5981–5987.
 (22) Zuccaccia, C.; Macchioni, A.; Orabona, I.; Ruffo, F. *Organometallics* **1999**, *18*, 4367–4372.
 (23) Yang, K.; Lachicotte, R. J.; Eisenberg, R. *Organometallics* **1998**, *17*, 5102–5113.
 (24) Scollard, J. D.; Labinger, J. A.; Bercaw, J. E., manuscript in preparation.
 (25) Brandow, C. G.; Zhong, H. A., unpublished results.

- (26) *The Chemist's Companion: A Handbook of Practical Data, Techniques, and References*; Gordon, A. J., Ford, R. A., Eds.; John Wiley & Sons: New York, 1972.

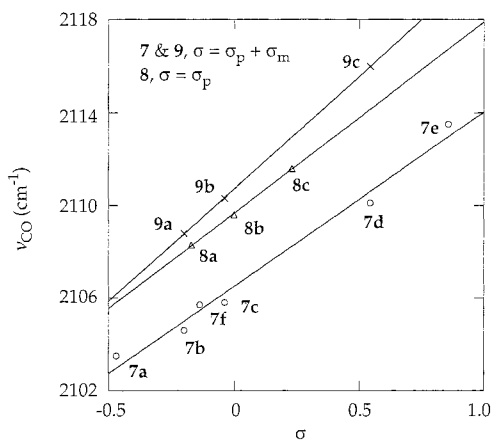


Figure 10. Plot of CO stretching frequencies for platinum(II) methyl carbonyl cations **7**, **8**, and **9** vs the σ values of the aryl substituents.

believe that the difference lies in steric factors; the 2,6-methyl groups in **8** cause the aryl groups to be oriented perpendicular to the coordination plane, minimizing crowding, whereas the less bulky aryls of **7** are rotated more parallel to the plane, in at least partial conjugation with the unsaturated $[N=C(\text{Me})-C(\text{Me})=N]$ group. This would be expected to result in more effective transmission of the substituent effects from the aryl group, via the diimine, to the metal center. AM1 semiempirical calculations²⁵ support this; free ligand **2b** is predicted to have the aryl ring locked perpendicular to the $[N-\text{Pt}-N]$ plane, with consequently little π -donation from the phenyl ring to the nitrogen atoms, while in **1f** the dihedral angle between the aryl ring and the diimine backbone is predicted to be approximately 60° , and the calculated electron density at the nitrogen in **1f** is higher than in **2b**.

Methyl substitution at backbone positions of the diimine ligands is also electron-releasing, as can be seen by comparing **7b-d** and **9a-c**, for which the aryl groups are identical; the CO stretching frequencies of the former (with backbone methyls) are red-shifted by about $4-6 \text{ cm}^{-1}$.

Ligand Electronic Effects on the Aquo/Solvento Equilibrium. All cations **10-12** generated by protonolysis of the corresponding dimethyl complexes with aqueous acid in TFE are formed as mixtures of solvento (*i*) and aquo (*ii*) adducts in rapid equilibrium (eq 5). In all cases measured, the equilibrium substantially favors the aquo adduct (Table 2). Furthermore, correlation of K_{eq} with ν_{CO} of the corresponding carbonyl cation shows that the preference for water over TFE increases as the metal center is made more electron-poor (Figure 11). This trend presumably reflects the greater electron-donating ability of water, relative to TFE, toward cationic Pt(II) centers. Similarly, the phenyl cations **17** and **18** are more selective toward water binding than the corresponding methyl cations **10** and **11**. Methyl groups are extremely good σ donors to metal centers, whereas phenyl groups are more electronegative (sp^2 - vs sp^3 -hybridized carbon) and thus less electron-donating, rendering the platinum center more electron-deficient.

Ligand Electronic Effects on Backbone Methyl Deuteration. In some cases, deuterium is incorporated into the backbone methyls of Pt(II) methyl acetonitrile adducts in $(\text{CD}_3)_2\text{CDOD}$, $\text{CD}_3\text{CD}_2\text{OD}$, and CD_3OD . This probably occurs via Lewis acid-catalyzed imine-enamine tautomerization (Scheme 9), whose rate will depend on both the basicity of the solvent and the acidity of the imine α -methyl proton.

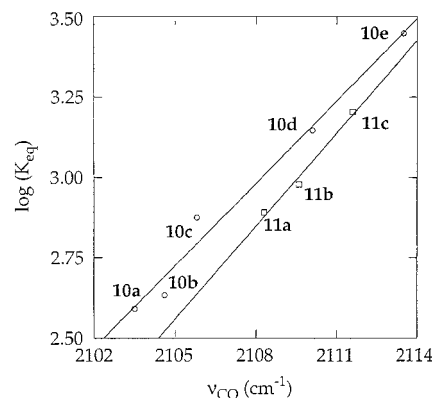
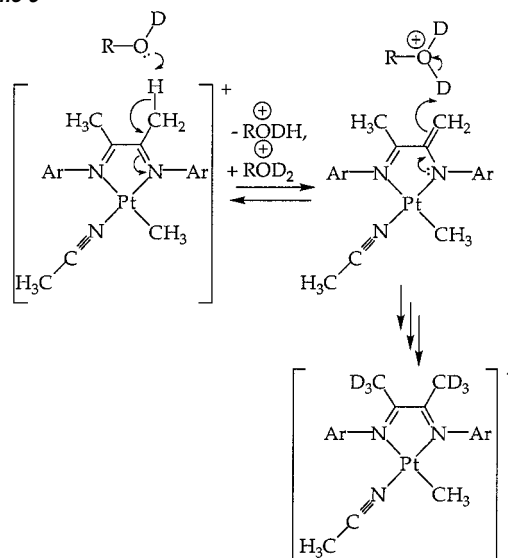


Figure 11. $\log(K_{\text{eq}})$ of **10** and **11** vs the CO stretching frequencies of the corresponding methyl carbonyl cations **7** and **8**.

Scheme 9



The basicity of alcohols decreases in the order $\text{Me}_2\text{CHOH} > \text{EtOH} > \text{MeOH} \gg \text{TFE}$, consistent with the observation that deuteration occurs fastest in deuterated 2-propanol and slowest in TFE- d_3 . Electron-withdrawing groups will increase the acidity of α -methyl protons, so the more electron-withdrawing diimine ligands should lead to a higher rate for deuterium incorporation into the methyl backbone. The more rapid exchange for **13d** than for **13b** is thus consistent with the higher ν_{CO} for **7d** than **7b**. The observation of exchange for **7e** even in TFE- d_3 at room temperature reflects the greater electron-withdrawing power of CO relative to acetonitrile.

The differential deuteration rates observed for the two backbone methyl groups in the same molecule may be attributed to the differing trans influence of methyl versus MeCN. Thus a Pt-N bond trans to MeCN is expected to be shorter, resulting in stronger donation to platinum, making the nitrogen more electropositive and accelerating exchange at the neighboring methyl group.

Ligand Effects on Overall Reaction Rates of Arene C-H Bond Activation. Pt(II) methyl cations **10-12** react cleanly with benzene to give the corresponding phenyl cations **17-19**, accompanied by liberation of methane. The kinetics are conveniently followed by ^1H NMR and exhibit clean first-order behavior in $[\text{Pt}]$. At sufficiently high water concentrations, where the Pt(II) aquo adducts account for $>90\%$ of the total platinum

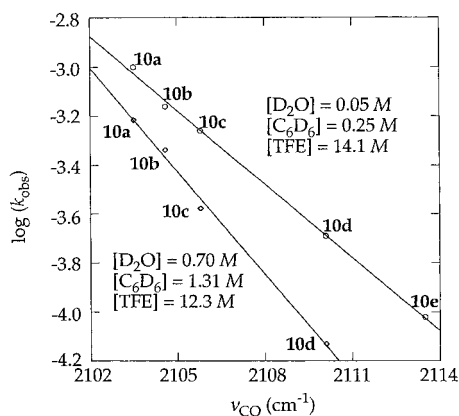


Figure 12. A plot of the logarithms of the observed rate constants in reactions of methyl cations **10** with C_6D_6 as a function of ν_{CO} of the corresponding methyl/carbonyl cations **7**.

species, the dependence on concentrations of benzene and water satisfy the apparent rate law: $\text{rate} = k_{\text{obs}}[\text{benzene}]/[\text{water}]$. A series of comparative experiments was performed to determine and distinguish ligand electronic and steric effects on k_{obs} .

The reaction rates of C_6D_6 with cations **10** were measured at 20 °C under two sets of conditions. At the lower water concentration ($[D_2O] = 0.05$ M, $[TFE-d_3] = 14.1$ M, and $[C_6D_6] = 0.25$ M), both the aquo and the solvento complexes are observed in the reaction mixtures, and at the higher water concentration ($[D_2O] = 0.70$ M, $[TFE-d_3] = 12.3$ M, and $[C_6D_6] = 1.31$ M), the aquo complexes are the only observable species. The logarithms of the observed rate constants are plotted against the IR CO stretching frequencies of the corresponding carbonyl complexes (**7**) in Figure 12. Under either set of reaction conditions, a good linear correlation is obtained, demonstrating that the more electron-rich Pt(II) cations are *more* reactive toward C_6D_6 . The slope of the linear correlation does depend on conditions, however. A similar correlation is found for cations **11** reacting with C_6D_6 at 35 °C (Figure 13a) and for cations **12** at 20 °C (Figure 13b).

The steric effects of the diimine ligands have a profound effect on the reactivity of the metal center. For example, **8a** has a CO stretching frequency of 2108 cm^{-1} , indicating that the corresponding **11a** is somewhat more electron-rich than **10d**, whose corresponding methyl-carbonyl cation **7d** has an IR stretching frequency of 2110 cm^{-1} . However, under the same reaction conditions, **10d** reacts an order of magnitude faster with C_6D_6 than does **11a** (Figure 14a). In general, reactions of benzene with complexes containing 2,6-dimethyl-substituted aryls (**11**) are considerably slower than those with no such substitution (**10**), indicating a substantial slowing effect of increasing steric bulk. On the other hand, Figure 14a indicates that the reactions of complexes **12** are considerably slower than those of **10** with similar electron density, although **12** should be, if anything, *less* crowded than **10**. We do not currently have a fully satisfying explanation for this apparent anomaly (*vide infra*).

Details of the Mechanism of Benzene C–H Bond Activation. The mechanism proposed previously to account for the reaction of benzene with **11b** is shown in Scheme 10.

The observed rate law, particularly the inverse dependence on water concentration, can be interpreted in terms of either a dissociative or a solvent-assisted associative pathway, but several considerations (to be discussed later) lead to a strong preference

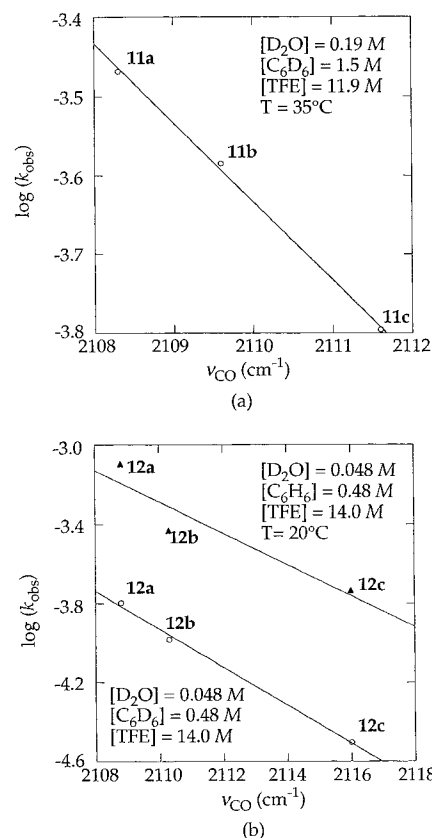


Figure 13. (a) A plot of the logarithms of the observed rate constants for reactions of cations **11** with C_6D_6 as a function of ν_{CO} for the corresponding methyl/carbonyl cations **8**. (b) A plot of the logarithms of the observed rate constants for reactions of cations **12** with C_6D_6/C_6H_6 as a function of ν_{CO} for the corresponding methyl/carbonyl cations **9**.

for the latter, so we will use Scheme 11 as the framework for our discussion.

In this scheme, the aquo (**Aii**) and solvento (**Ai**) complexes are in rapid equilibrium, with benzene displacing the more weakly bound solvent ligand; direct attack of benzene on **Aii** to displace water is assumed to be negligible, although a small contribution from this route would probably not perturb the kinetics enough to be detectable. π -Benzene complex **B** then undergoes C–H bond cleavage (probably via a σ -complex **C**). Limiting cases for the rate-determining step would be formation of **B** ($k_2 > k_{-1}[TFE]$) or C–H cleavage ($k_2 < k_{-1}[TFE]$). In either case, the deduced rate law (see Supporting Information for derivation) predicts that a plot of $1/k_{\text{obs}}$ versus $[H_2O]/[C_6H_6]$ will be linear, which is observed in all cases (Figure 3). At high water concentrations ($K_{\text{eq}}[H_2O] \gg [TFE]$), the water complex **Aii** is the major species in solution, and a plot of k_{obs} versus $[C_6H_6]/[H_2O]$ is expected to be linear, as long as benzene and water are not present in high enough concentrations to significantly alter the solvent properties. This expectation is born out by the experimental results. At low water concentrations ($K_{\text{eq}}[H_2O] \approx [TFE]$), concentrations of **Ai** and **Aii** will both be significant, so a plot of k_{obs} versus $[C_6H_6]/[H_2O]$ would be expected to deviate from linearity, as observed.

For **11b**, formation of π -benzene adduct **B** was inferred to be the rate-determining step, primarily on the basis of the first-order dependence on benzene concentration coupled with the low KIE (~ 1) and the virtually complete isotopic scrambling observed (see below).¹¹ It is of interest here to compare the

Scheme 10

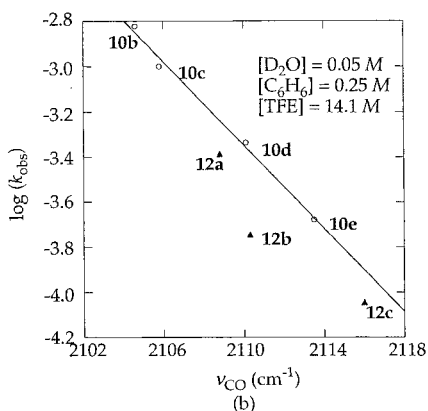
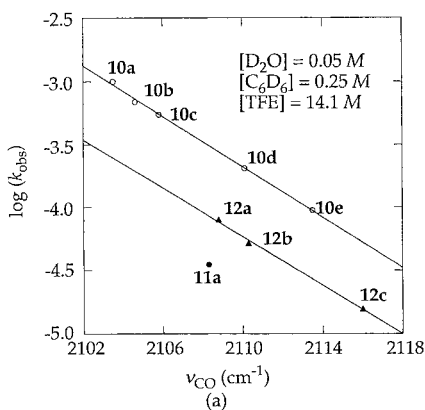
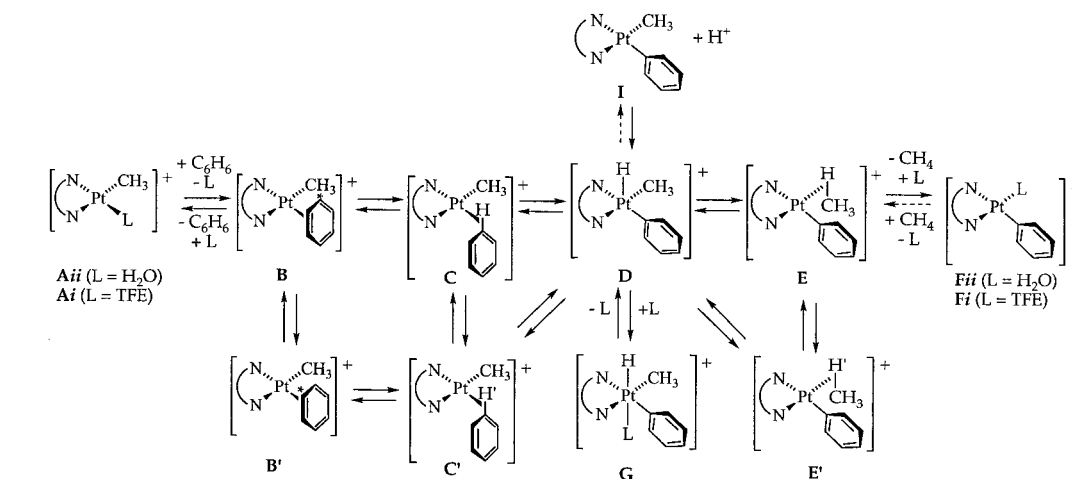


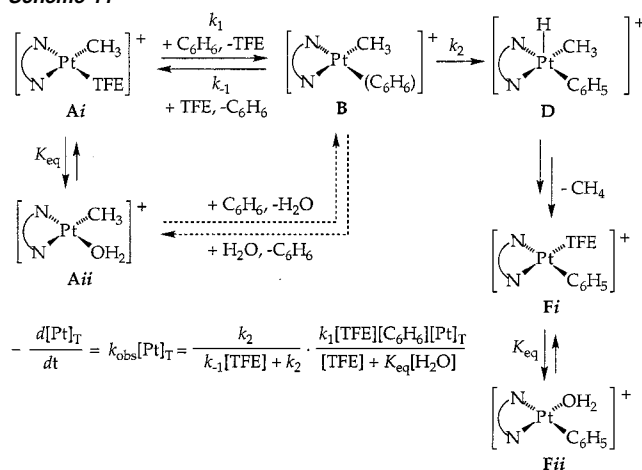
Figure 14. (a) A plot of the logarithms of the observed rate constants in reactions of Pt(II) cations of variable steric bulk with C_6D_6 as a function of ν_{CO} . (b) A plot of the logarithms of the observed rate constants in reactions of Pt(II) cations of variable steric bulk with C_6H_6 as a function of ν_{CO} .

behavior of cations **10** (which lack 2,6-dimethyl substituents on the aryl groups) with that previously found for **11b** (as well as the new findings for **11a** and **11c**). While the two series appear quite similar in some regards, particularly with respect to one major trend, the dependence of reactivity on electronic character, other phenomena appear quite different. In the next few sections, we will try to account for and reconcile both the differences and the similarities within the basic framework of Scheme 10.

Isotopic Exchange and Kinetic Deuterium Isotope Effects.

It should first be noted that no discernible amount of deuterium is detected in the methane liberated from the reaction between

Scheme 11

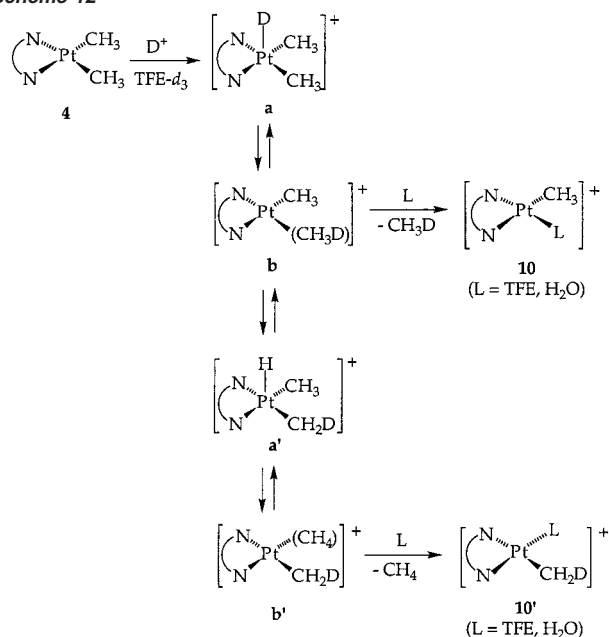


any complex and C_6H_6 in TFE- d_3 . This means that reversible deprotonation of intermediate **D** (to give **I**) in Scheme 10 is much slower than all other reactions, since otherwise deuterium from solvent would exchange into the complex and thence into the methyl group. Furthermore, the fact that no H/D exchange occurs in the present system explains the observation that when cations **10** are generated by protonolysis of **4** in TFE- d_3 , only [Pt- CH_2D] and [Pt- CH_3] complexes are formed, with corresponding amounts of CH_4 and CH_3D ; no multiple deuteration is detectable. As shown in Scheme 12, addition of D^+ (from aqueous DBF_4) to the platinum dimethyl complexes gives a Pt(IV)-D species **a**, which undergoes C-D bond formation to form **b**, which may either directly release CH_3D to afford **c** or rearrange and cleave a C-H bond to yield **a'**.

Because there is no H/D exchange between the solvent and Pt(IV) hydrido intermediates, only one deuterium atom is involved for each molecule of methane released. This deuterium atom is either incorporated into the liberated methane as CH_3D or left behind as [Pt- CH_2D]. This stands in contrast to previous protonolysis studies of Pt(II) alkyl complexes in CD_3OD , where substantial deuterium incorporation into the Pt alkyl group was observed.⁵ The difference may reflect the reduced basicity of TFE as compared to that of methanol.

If the rate of the scrambling process in Scheme 12 is fast relative to the loss of methane, a statistical mixture of CH_3D and CH_4 (4:3) will be obtained (assuming negligible KIE for C-H vs C-D activation and methane dissociation); if the

Scheme 12



reverse is true, only CH_3D will be produced. As Figure 1 shows, for **4b** the ratio of CH_3D to CH_4 increases with increasing acetonitrile concentration, implying that elimination of methane is associative. Similar observations for **4e** and **5b** have been reported recently by Tilset and co-workers.²⁷

When cations **10** are treated with C_6D_6 , the liberated methane includes isotopomers with more than one deuterium atom. This is consistent with the mechanism of Scheme 10, if reversible interconversions among intermediates **C–E** and the accompanying rearrangements to **C'** and **E'** occur at a rate at least comparable to those of dissociation of methane from **E** and **C**. However, in contrast to **11b**, where isotope scrambling between the methane and platinum-phenyl groups is essentially statistical,¹¹ for **10** a much smaller degree of scrambling is found. The ratio of approximately 2:1 $\text{CH}_3\text{D}:\text{CH}_2\text{D}_2$ for **10b** indicates that **E** loses methane on the order of twice as fast as it reverts to **C**.

Up to 20% of the unreacted starting material becomes deuterated, giving $[\text{Pt}-\text{CH}_2\text{D}]$, during reactions between **10** and C_6D_6 , which implies that some of the time intermediate **E**, which will have coordinated CH_3D after a single C–H activation/cleavage sequence, reverts all the way back to starting materials. The relatively low levels of deuterium incorporation into the platinum methyl group are consistent with the previous finding, on the basis of protonolysis of a mixed $[\text{Pt}(\text{Me})(\text{Ph})]$ complex, that the rate for benzene elimination is $\sim 4\text{--}5$ times slower than that of methane elimination, which translates to a $\Delta\Delta G^\ddagger$ of $\sim 0.8\text{--}0.9$ kcal mol⁻¹ at room temperature.¹¹ This observation also implies that some of the evolved methane will come from complexes that have interacted with more than one molecule of C_6D_6 , which may have consequences for KIE measurements (vide infra).

Kinetic deuterium isotope effects (KIEs) were measured for all complexes **10–12** by comparing the rates of disappearance of starting material in the presence of C_6H_6 versus those with C_6D_6 under otherwise identical conditions. The most striking observation in Table 3 is the difference in behavior between

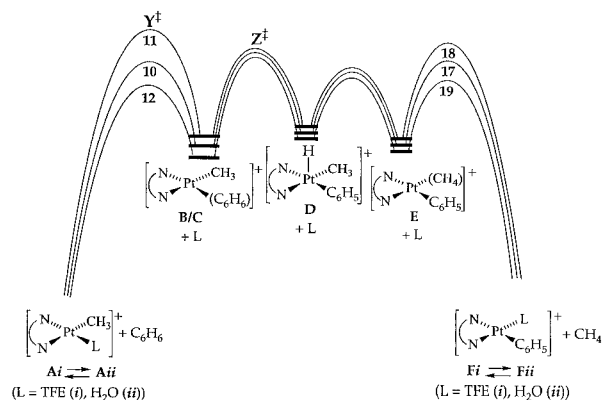


Figure 15. Reaction coordinate for reactions between **10**, **11**, **12** and benzene.

complexes **10** and **11**: the former have KIE values around 2, while the latter are close to unity. For several examples of **10**, we also measured the KIEs by intermolecular (1:1 $\text{C}_6\text{H}_6:\text{C}_6\text{D}_6$) and intramolecular (1,3,5- $\text{C}_6\text{H}_3\text{D}_3$) competition reactions; this approach would be much more complicated (by intermolecular competition) or impossible (by intramolecular competition) for **11** because of the near-statistical isotope scrambling. We find that the KIEs measured from the competition reactions are slightly, but consistently, smaller than those measured by parallel reactions. This observation may be accounted for by the fact that more than one molecule of benzene may be involved in the reaction (vide supra) (Scheme 10). Thus, for example, in an intermolecular competition reaction of **10** with C_6D_6 or C_6H_6 , initial C_6D_6 activation followed by complete reversion to starting material accompanied by deuterium incorporation into $[\text{Pt}-\text{CH}_3]$ happens occasionally; the subsequent conversion to **17** will give deuterated methane even if it involves C_6H_6 . In the parallel method, such a sequence (participation of more than one benzene molecule) will have no consequences, since only rates and not degrees of deuteration are measured. Thus the competitive method overestimates the apparent relative frequency of C_6D_6 activation.

The differences between **10** and **11** in behavior for both isotope exchange and KIE are explicable in terms of Figure 15, analogous to Scheme 10 but with the assumption of a change in the rate-determining step. For **10**, to account for a significant KIE, the rate-determining step must involve the C–H (C–D) bond: either the actual C–H cleavage step, **C** \rightarrow **D**, or (less likely) the coordination of the C–H bond, **B** \rightarrow **C**. That would also explain the relatively low level of isotopic exchange, as the barrier to dissociation of benzene from **B** (and, by extension, that of methane from **E**) must be lower than at least one barrier within the manifold of reactions that effect such exchange. This case is represented by the free energy profile for **10** \rightarrow **17** in Figure 15. The highest point on the energy surface is transition state **Z**[‡].

In contrast, for **11** the highest point on the surface must be transition state **Y**[‡], which governs the initial coordination of benzene. Since this coordination involves a π bond of benzene, no primary KIE at all would be anticipated. Furthermore, the complete statistical isotope exchange implies that once the manifold of intermediates **C–E** has been entered, loss of benzene or methane is much slower than interconversions among those intermediates. The differences in entropy of activation, strongly negative for **11b**, very small for **10b**, also seem

(27) Johansson, L.; Tilset, M. *J. Am. Chem. Soc.* **2001**, *123*, 739–740.

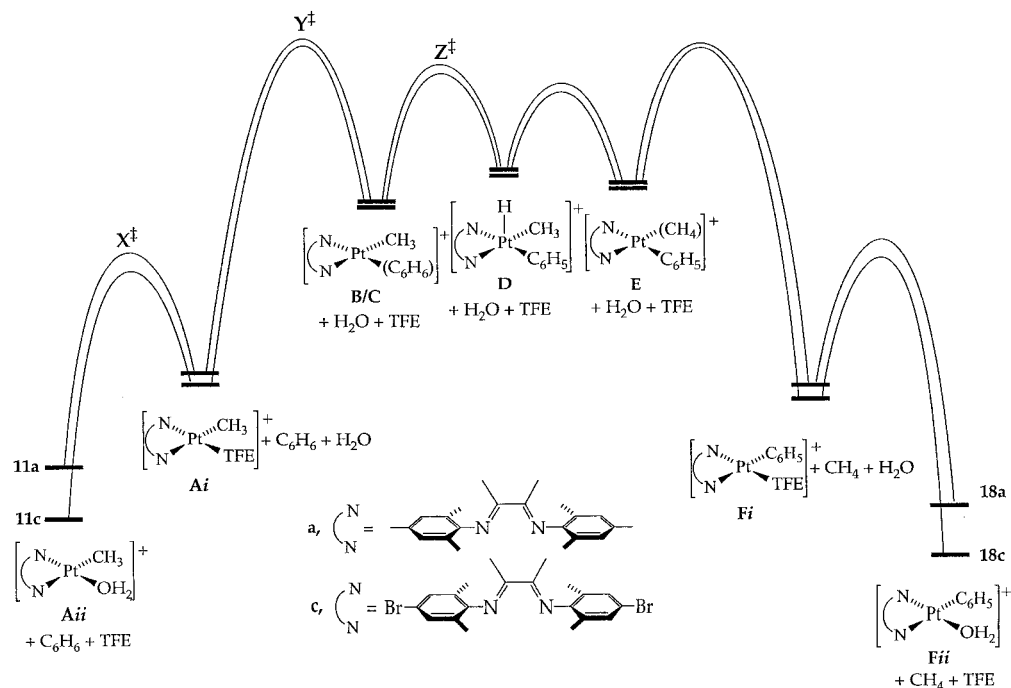


Figure 16. Reaction coordinate for reactions between **11a** and **11c** and benzene, showing that the differences in rate within a series arise from ground-state energy differences for the aquo/methyl cations (**Aii**). Similar profiles apply to **10** and **12**, with the highest energy transition states being **Z[‡]**, not **Y[‡]**.

consistent with the former, but not the latter, involving rate-determining associative (vide infra) substitution.

Why should this rate-determining step switch operate? A steric explanation appears the most probable. Coordination of benzene in η^2 -C,C mode places the benzene molecule right in the coordination plane, subject to steric interactions with the other ligands. For **11**, with 2,6-dimethyl-substituted aryl groups, these interactions can be expected to be more significant than for **10**, which has no substituents in the 2,6-positions. Hence in **11** there will be relative destabilization of both the intermediate **B** itself and, presumably, the transition state (**Y[‡]**) leading thereto, as compared to **10**.

The KIEs for **12** are considerably larger than those for **10** (3.6–5.9 vs ~ 2). One might argue that **12** is even less sterically crowded than **10**, by virtue of the missing backbone methyl groups, which would lower transition state **Y[‡]** still further (Figure 15). This might suggest that **12** gives a better measure of the inherent KIE for rate-determining C–H bond activation, whereas for **10** the energies of **Y[‡]** and **Z[‡]** are sufficiently close that C–H activation is not *completely* rate-determining, and the measured KIE values are hybrids. However, given that the rates of the reactions of **12** with benzene are slower than steric considerations would lead us to expect, this conclusion must remain tentative for the present.

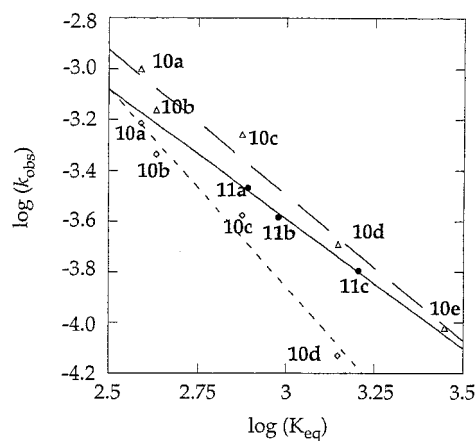
Electronic Effects on Rates. Within each series **10–12** the changes in substituents (in the 3,5-positions for **10** and **12** and in the 4-positions for **11**) are far enough removed from the metal center that steric parameters should change little, and thus the observed trend within each series should reflect a purely electronic effect. For both series, as the Pt(II) centers become more electron-rich (as measured by lower CO stretching frequencies in the analogous carbonyl cations), benzene C–H bond activation becomes faster. In principle, this trend could be explained in a number of ways. For cations **10** and **12**, for example, one might argue that (1) C–H activation is the rate-

determining step; (2) the intermediates **D** thus formed are formally Pt(IV), more electron-deficient than the Pt(II) cations; and (3) the transition state **Z[‡]** leading to that intermediate should have at least partial higher oxidation state character. Hence more strongly electron-donating ligands can better stabilize the higher oxidation state intermediates/transition states and accelerate the reaction.

On the other hand, a closely parallel trend is observed also for cations **11**, for which C–H bond activation does *not* appear to be rate-determining, but rather the replacement of TFE solvent by benzene. It is conceivable that the replacement might coincidentally follow the same order; that is, that transition state **Y[‡]** is also stabilized by electron-donating ligands. While acetonitrile self-exchange rates follow the opposite trend, faster at more electron-deficient metal centers (vide infra), the electronic demands for the coordination of benzene versus acetonitrile as the displacing ligand might well be different. However, it would be much more satisfying to find a single explanation that accounts simultaneously for all the series.

Since the transition states for the series appear to be quite different, the simplest explanation for common behavior is that we are dealing primarily with a ground-state effect. That is, the most important effect of changing the electronic properties of the diimine ligand is upon the relative stability of the aquo complexes $[(\text{ArN}=\text{CR}-\text{CRN}=\text{Ar})\text{Pt}(\text{Me})(\text{H}_2\text{O})]^+$ ($\text{R} = \text{Me}$ or H , **Aii** in Scheme 10). If the energies of either of the transition states **Y[‡]** or **Z[‡]** are less sensitive to changes in the diimine ligand than that of **Aii**, then the rates of benzene activation by series **10/12** and **11** will exhibit the same trend even though they have different rate-determining steps (shown for series **11** in Figure 16; similar profiles would be obtained for **10** and **12**, with the highest energy transition states being **Z[‡]**, not **Y[‡]**).

If we further postulate that the same is true for the energy of solvento complex **Ai**, then the equilibrium constants between **Aii** and **Ai** would be expected to vary with ligand in much the



Symbol	Complex	Temp. (°C)	[C ₆ D ₆] (M)	[D ₂ O] (M)	[TFE-d ₃] (M)
---△---	10	20	0.25	0.05	14.1
—●—	11	35	1.50	0.19	11.9
---○---	10	20	1.30	0.70	12.3

Figure 17. A log–log plot of the observed rate constants between C₆D₆ and methyl cations **10** and **11** vs the aquo/solvento equilibrium constants for the corresponding methyl solvento \rightleftharpoons aquo cations **10i** \rightleftharpoons **10ii** and **11i** \rightleftharpoons **11ii**.

same way as the rate constants. This is in fact the case, as shown in Figure 17; the plots of $\log(k_{\text{obs}})$ versus $\log(K_{\text{eq}})$ give reasonably straight lines, with slope close to unity, for the three sets of data.

While this interpretation is consistent with the most prominent features of the ligand–reactivity relationship, it is far from conclusive, and some observations remain unexplained, particularly the low reactivity of **12**. Figure 14 shows that both **12b** and **11a** are less reactive than **10d**, though all have comparable electron density. The difference between **11a** and **10d** can be explained on steric grounds as the former has 2,6-dimethyl-substituted aryl groups, but **12b** should be, if anything, less crowded than **10d**. Apparently the replacement of backbone methyl groups with hydrogens has an additional, as yet unexplained effect here, as well as on the KIEs (vide supra).

Acetonitrile Exchange. A rate expression of $k_{\text{ex}} = k_1 + k_2[\text{CD}_3\text{CN}]$ has been obtained for acetonitrile isotopic exchange reactions. The k_1 term could represent either a unimolecular dissociative pathway or a solvent-assisted associative pathway. The highly negative entropy of activation for the k_1 term seems inconsistent with a dissociative pathway and indicative of a solvent-assisted pathway, though this is not definitive; solvation of the cations can play an important role. However, both terms exhibit similar entropies of activation, suggesting that both pathways operate by the same mechanism. That is, the isotopic acetonitrile exchange consists of both a solvent-assisted associative pathway and a direct attack associative pathway.

Although the k_1 values vary considerably as the solvent is changed from methanol to ethanol to 2-propanol, when divided by bulk solvent concentrations the resulting k_s values are all about the same (Table 3). Apparently the solvent term is not very sensitive to the steric bulk of the solvent. On the other hand, k_1 for TFE is essentially zero, presumably reflecting the very low basicity of that solvent. The second-order rate constants for direct acetonitrile attack (k_2) do vary across the entire set of

alcohols, probably due to differences in solvation energies of the cations.²⁸

Table 5 shows that the more electron-poor complexes (**13d** vs **13b**, **14c** vs **14b**) exhibit higher exchange rate constants for both the solvent-assisted (k_s) and direct (k_2) terms. This is the opposite trend from that found for benzene activation and probably indicates stabilization of a five-coordinate transition state in the associative substitution. The most closely corresponding species in Figure 16 would be the transition state for substitution of water by TFE (X^+); note that the energy of that species has *no consequence whatsoever* on the rate of benzene activation, if the arguments represented by that energy diagram are correct. Hence there is no inconsistency between the two opposing trends. Comparison of acetonitrile exchange for **14b** and **13d** (whose corresponding carbonyl cations have very similar ν_{CO} values) reveals a moderate steric effect as well, around a factor of 4, not quite so large as the steric retardation that appears to operate in benzene activation.

Reactions of Alkylaromatics. Our results combined with those of Tilset²⁰ suggest an inherent reactivity preference for aromatic over benzylic C–H activation, which can however be readily overridden by steric effects. Thus the relatively uncrowded **10b** reacts with *p*-xylene to give **20b**, the product of reaction at an aryl C–H, whereas more crowded **11b** gives primarily benzylic activation. With mesitylene, still more sterically encumbered, **10b** gives a mixture of products, somewhat favoring benzylic activation (**21b**), and the aromatic activation product **22b** appears, from its accelerated decomposition to ($\mu\text{-OH}$)₂ dimer **16b**, to be significantly destabilized. The substrate-derived crowding in these two cases may also cause a shift to rate-determining (or partially so) substrate coordination, as the KIEs decrease significantly with steric bulk.

The C–H activation chemistry of purely aliphatic hydrocarbons will be reported later.²⁹

Conclusions

The results reported here, combined with some earlier findings, support three main conclusions: (1) For the reaction of benzene with cationic Pt(II) complexes bearing 3,5-disubstituted aryl diimine ligands (**10**), the rate-determining step is C–H bond activation; whereas for the more sterically crowded analogues with 2,6-dimethyl-substituted aryl groups (**11**), benzene coordination becomes rate-determining. This switch is manifested in distinctly different isotope scrambling and KIE patterns. (2) The more electron-rich the ligand is, as assayed by the CO stretching frequency of the corresponding carbonyl cationic complex, the faster the rate of C–H bond activation. This at first sight appears to be at odds with the common description of this class of reaction as electrophilic. However, the fact that the same trend is observed for the two different series of complexes, which have different rate-determining steps, suggests that this finding does not reflect the actual C–H bond activation process, but rather reflects only the relative ease of benzene displacing a ligand to initiate the reaction, which in turn appears to be mostly a ground-state effect. It is hence not possible to say much, if anything, about the “inherent” nature of C–H activation on the basis of these results. (3) Several lines of evidence suggest that associative substitution pathways operate

(28) Romeo, R.; Minniti, D.; Lanza, S. *Inorg. Chem.* **1980**, *19*, 3663–3668.

(29) Zhong, H. A.; Labinger, J. A.; Bercaw, J. E., unpublished results.

here to get the hydrocarbon substrate into, and out of, the coordination sphere. While associative substitution does predominate in the chemistry of square-planar Pt(II), there are situations where dissociative mechanisms become preferred,³⁰ and one might think that the present cases, involving (presumably) very weakly bonded arenes and alkanes, would fall into that category. However, acetonitrile exchange seems to be clearly associative. More to the point, the fact that addition of acetonitrile, a better nucleophile than solvent TFE, suppresses isotopic scrambling between benzene and methyl groups strongly implies that the replacement of coordinated methane is associative. Analogous behavior has recently been observed for the displacement of coordinated arenes.²⁰ From the principle of microscopic reversibility, we infer that the displacement of solvent (water, acetonitrile) by hydrocarbon also proceeds associatively.

The implications of these findings with respect to the ultimate goal, the development of a practical, selective alkane functionalization catalyst, remain the subject of ongoing research in our labs.

Experimental Section

General Considerations. All moisture-sensitive compounds were manipulated using standard vacuum line, Schlenk or cannula techniques, or in a drybox under a nitrogen atmosphere. Argon and dinitrogen gases were purified by passage over columns of MnO on vermiculite and activated molecular sieves. Trifluoroethanol was purchased from Aldrich, purified and dried over a mixture of CaSO₄/NaHCO₃, then either vacuum distilled or distilled under argon and stored over activated molecular sieves under vacuum. Trifluoroethanol-*d*₃ was purchased from Aldrich, stored over activated molecular sieves and a small amount of NaHCO₃ under vacuum, and vacuum distilled into oven-dried J-Young NMR tubes for kinetic studies. Benzene and benzene-*d*₆ were vacuum distilled from sodium benzophenone ketyl shortly before kinetic runs and stored over activated molecular sieves. Toluene was vacuum distilled from sodium benzophenone ketyl. Triethylamine was distilled from CaH₂ and stored under Ar. 3,5-di-*tert*-butyl-4-methoxyaniline and the corresponding diimine ligand **1a** were synthesized by Dr. Joseph Sadighi. Bis(dimethyl(μ -dimethyl sulfide)platinum(II)) was prepared according to literature procedure.¹⁷ All other solvents and reagents were used as received without further purification.

NMR spectra were recorded on a GE QE300 (¹H, 300.1 MHz), a Varian INOVA 500 (¹H, 499.852 MHz, ¹³C, 125.701 MHz), or a Varian Mercury 300 (¹H, 299.8 MHz, ¹⁹F, 282.081 MHz, ¹³C, 75.4626 MHz) spectrometer. IR spectra were recorded on a Perkin-Elmer 1600 series FTIR spectrometer. Mass spectra were measured on a Micromass LCT instrument with a Z-spray source at University of California Irvine, using electrospray orthogonal acceleration time-of-flight technique. Under the analytical conditions, protonolysis occurs at the platinum center in the platinum dimethyl complexes **4–6**, which were consequently detected as the cationic species [(N–N)Pt(Me)(NCMe)]⁺ (NCMe was the solvent used in the analysis). Elemental analyses were performed at Midwest MicroLab LLC. A number of samples gave analytical results lower than the expected values (these were generally very small samples that may have been contaminated with either a small amount of silica (from the filtration frit on which they were isolated) or TFE solvent), but all analyzed correctly in the electrospray mass spectrum.

1,4-Bis(3,5-di-*tert*-butylphenyl)-2,3-dimethyl-1,4-diaza-1,3-butadiene (^tBu₂ArDAB^{Me}, **1b**). 3,5-Di-*tert*-butylaniline (0.9732 g, 4.74 mmol) and 2,3-butanedione (0.204 g, 2.36 mmol) were dissolved in 15 mL of

MeOH. To this yellow solution, two drops of formic acid were added, and a very pale yellow precipitate formed within 15 min. The mixture was stirred at room temperature for 14 h, cooled, filtered, washed with cold methanol (2 × 5 mL), and dried over an aspirator for 3 h. **1b** was isolated as an extremely pale yellow powder (0.95 g, 87%). ¹H NMR (500 MHz, C₆D₆): δ = 1.32 (s, 36H, C(CH₃)₃), 2.33 (s, 6H N=C–CH₃), 6.90 (d, ⁴J_{H–H} = 1.8 Hz, 4H, Ar-*H*), 7.35 (t, ⁴J_{H–H} = 1.8 Hz, 2H, Ar-*H*). ¹³C {¹H} NMR (125 MHz, C₆D₆): δ = 15.78 (N=C–CH₃), 31.97 (C(CH₃)₃), 35.40 (C(CH₃)₃), 114.27 (*o*-Ar–C), 118.19 (*p*-Ar–C), 151.860, 152.24 (Ar–C), 168.57 (N=C–CH₃). ESMS, Calcd for C₃₂H₄₈N₂H ([M + H]⁺): 461.3896. Found: 461.3906.

1,4-Bis(3,4,5-trimethoxyphenyl)-2,3-dimethyl-1,4-diaza-1,3-butadiene (^{OMe}ArDAB^{Me}, **1c**). 3,4,5-Trimethoxyaniline (0.9875 g, 5.39 mmol) and 2,3-butanedione (0.225 g, 2.61 mmol) were dissolved in 30 mL of MeOH. To this yellow solution was added several drops of formic acid, and a bright yellow precipitate formed overnight. The mixture was stirred at room temperature for 14 h, cooled, filtered, washed with cold methanol (2 × 5 mL), and dried over an aspirator for 3 h. **1c** was isolated as a bright yellow powder (0.757 g, 70%). ¹H NMR (500 MHz, C₆D₆): δ = 2.32 (s, 6H, N=C–CH₃), 3.40 (s, 12H, OCH₃), 3.90 (s, 6H, OCH₃), 6.19 (s, 4H, Ar-*H*). ¹³C {¹H} NMR (125 MHz, C₆D₆): δ = 15.91 (N=C–CH₃), 56.15 (OCH₃), 61.06 (OCH₃), 97.46 (*o*-Ar–C), 136.26, 147.90, 155.06 (Aryl C's), 169.04 (N=C–CH₃). ESMS, Calcd for C₂₂H₂₈N₂O₆Na ([M + Na]⁺): 439.1845. Found: 439.1848.

1,4-Bis(3-methoxy-5-(trifluoromethyl)phenyl)-2,3-dimethyl-1,4-diaza-1,3-butadiene (^{OMeCF₃Ar}DAB^{Me}, **1d**). 3-Methoxy-5-(trifluoromethyl)aniline (1.27 g, 6.65 mmol) and 2,3-butanedione (0.286 g, 3.32 mmol) were dissolved in 30 mL of MeOH. To this yellow solution was added several drops of formic acid, and the mixture was stirred at room temperature for 2 days without forming any precipitation. The volatiles were then removed on a rotavap, and 6.8 g of activated 5 Å molecular sieves were added to a toluene solution of the above residues. The mixture was heated at 80–90 °C for two nights. The molecular sieves were then filtered away and washed with methylene chloride (4 × 10 mL). The volatiles were evaporated, and 20 mL of methanol was added to the residue. After stirring at room temperature for an hour, the insolubles were collected, washed with cold methanol (2 × 5 mL), and dried over an aspirator for 3 h. **1d** was isolated as an off-white powder (0.75 g, 52%). ¹H NMR (500 MHz, C₆D₆): δ = 1.90 (s, 6H, N=C–CH₃), 3.13 (s, 6H, OCH₃), 6.43 (m, 2H, Ar-*H*), 6.72 (m, 2H, Ar-*H*), 6.90 (m, 2H, Ar-*H*). ¹³C {¹H} NMR (125 MHz, C₆D₆): δ = 15.52 (N=C–CH₃), 55.33 (OCH₃), 106.38 (³J_{C–F} = 3.8 Hz, Ar–C), 108.67 (²J_{C–F} = 3.67 Hz, Ar–C), 108.79 (⁴J_{C–F} = 0.98 Hz, Ar–C), 125.63 (¹J_{C–F} = 270.35 Hz, CF₃), 133.17 (²J_{C–F} = 32.3 Hz, Ar–C), 153.56, 161.52 (Ar–C), 169.34 (N=C–CH₃). ¹⁹F NMR (282 MHz, C₆D₆): δ = –64.81. ESMS, Calcd for C₂₀H₁₈N₂O₂F₆H ([M + H]⁺): 433.1351. Found: 433.1357.

1,4-Bis(2,4,6-trimethylphenyl)-2,3-dimethyl-1,4-diaza-1,3-butadiene (^{Me₃Ar}DAB^{Me}, **2a**). 2,4,6-Trimethylaniline (13.521 g, 100 mmol) and 2,3-butanedione (4.307 g, 50 mmol) were dissolved in 50 mL of MeOH. To this yellow solution was added several drops of formic acid, and a bright yellow precipitate formed overnight. The mixture was stirred at room temperature for 24 h, filtered, washed with methanol (2 × 5 mL), and dried over an aspirator for 4 h. **2a** was isolated as a bright yellow powder (14.78 g, 92%). ¹H NMR (500 MHz, C₆D₆): δ = 2.00 (s, 12H, *o*-CH₃), 2.07 (s, 6H, *p*-CH₃), 2.22 (s, 6H, N=C–CH₃), 6.85 (s, 4H, Ar-*H*). ¹³C {¹H} NMR (125 MHz, C₆D₆): δ = 16.08 (N=C–CH₃), 18.24 (*o*-CH₃), 21.21 (*p*-CH₃), 124.91 (*o*-Ar–C), 129.44 (*m*-Ar–C), 132.70 (*p*-Ar–C), 147.09 (ipso-Ar–C), 168.76 (N=C–CH₃). ESMS, Calcd for C₂₂H₂₈N₂H ([M + H]⁺): 321.2331. Found: 321.2323.

1,4-Bis(2,6-dimethyl-4-bromo-phenyl)-2,3-dimethyl-1,4-diaza-1,3-butadiene (^{Me₂BrAr}DAB^{Me}, **2c**). To a mixture of 2,6-dimethyl-4-bromoaniline (5.103 g, 25.5 mmol) and 2,3-butanedione (1.078 g, 12.52 mmol) was added 100 mL of methanol. The aniline was not very soluble in methanol. To this yellow solution was added several drops of formic

(30) Romeo, R. *Comments Inorg. Chem.* **1990**, *11*, 21–57.

acid. The mixture was stirred at room temperature for 48 h, filtered, and washed with methanol (5×5 mL). The filtrate was concentrated to ~ 30 mL, filtered, and washed. The insolubles were combined and dried over an aspirator for 4 h. **2c** was isolated as a pale yellow powder (4.84 g, 86%). $^1\text{H NMR}$ (500 MHz, C_6D_6): $\delta = 1.71$ (s, 12H, *o*- CH_3), 1.82 (s, 6H, $\text{N}=\text{C}-\text{CH}_3$), 7.14 (s, 4H, *Ar-H*). ^{13}C $\{^1\text{H}\}$ NMR (125 MHz, C_6D_6): $\delta = 16.02$ ($\text{N}=\text{C}-\text{CH}_3$), 17.78 (*o*- CH_3), 116.725 (*Br-Ar-C*), 127.33 (*o*-*Ar-C*), 131.449 (*m*-*Ar-C*), 148.11 (*ipso*-*Ar-C*), 168.84 ($\text{N}=\text{C}-\text{CH}_3$). ESMS, Calcd for $\text{C}_{20}\text{H}_{22}\text{N}_2\text{Br}_2\text{H}$ ($[\text{M} + \text{H}]^+$): 449.0228 (^{79}Br), 451.0209 (^{81}Br). Found: 449.0231, 451.0222.

1,4-Bis(3,5-di-*tert*-butylphenyl)-1,4-diaza-1,3-butadiene ($^{\text{tBu}_2\text{Ar}}\text{DAB}^{\text{H}}$, **3a**). Br_2 (0.25 mL, 4.85 mmol) was added to a 30 mL CH_2Cl_2 solution of PPh_3 (1.30 g, 4.96 mmol) at 0°C under Ar. After the red color disappeared, the solvent was removed by rotavap, leaving behind a white powder. A toluene solution of 3,5-di-*tert*-butylaniline (1.00 g, 4.87 mmol) was added to the above white powder under Ar to form an orange solution with white precipitate. Triethylamine (2 mL, 14.4 mmol) was added to the mixture, and the solution turned light yellow with more white precipitate appearing. The mixture was heated to $80-90^\circ\text{C}$ under argon, and the reaction was allowed to proceed overnight. After 14 h, the reaction flask was cooled to room temperature, the mixture was filtered to remove NET_3HBr , and the insolubles were washed with petroleum ether (3×20 mL). The filtrate was then concentrated, and dry heptane was added to the oily residues. The iminophosphorane (1.4 g, 62%) was isolated by recrystallization from heptane. $^1\text{H NMR}$ (300 MHz, C_6D_6): $\delta = 1.31$ (s, 18H, $\text{C}(\text{CH}_3)_3$), 6.9–7.1 (overlapping peaks, 12H, *Ar-H*), 7.80 (m, 6H, *Ar-H*). Dry THF was added to the iminophosphorane (1.05 g, 2.26 mmol), glyoxal trimer (77 mg, 0.37 mmol), and 1 g of 4 \AA molecular sieves under Ar, and the mixture was refluxed overnight. After cooling to room temperature, THF was removed, and the residue was dissolved in 10 mL of CH_2Cl_2 . The yellow solution was filtered through a pad of silica gel and Celite to remove triphenylphosphine oxide. The silica gel was washed with additional CH_2Cl_2 . All CH_2Cl_2 solution was combined, and the solvent was removed. MeOH was added to the residue, and the yellow insolubles were collected (350 mg, 72%). $^1\text{H NMR}$ (500 MHz, C_6D_6): $\delta = 1.27$ (s, 37H, $\text{C}(\text{CH}_3)_3$), 7.35 (d, $^4J_{\text{H-H}} = 1.5$ Hz, 4H, *Ar-H*), 7.48 (t, $^4J_{\text{H-H}} = 1.5$ Hz, 2H, *Ar-H*), 8.67 (s, 2H, $\text{N}=\text{C}-\text{H}$). ^{13}C $\{^1\text{H}\}$ NMR (125 MHz, C_6D_6): $\delta = 31.84$ ($\text{C}(\text{CH}_3)_3$), 35.38 ($\text{C}(\text{CH}_3)_3$), 116.38 (*o*-*Ar-C*), 122.188 (*p*-*Ar-C*), 151.60 (*ipso*-*Ar-C*), 152.622 (*m*-*Ar-C*), 160.18 ($\text{N}=\text{C}-\text{H}$). ESMS, Calcd for $\text{C}_{30}\text{H}_{44}\text{N}_2\text{H}$ ($[\text{M} + \text{H}]^+$): 433.3583. Found: 433.3584.

1,4-Bis(3,4,5-trimethoxyphenyl)-1,4-diaza-1,3-butadiene ($^{\text{OMe}_3\text{Ar}}\text{DAB}^{\text{H}}$, **3b**). The iminophosphorane was synthesized similarly starting with 3,4,5-trimethoxyaniline (2 g, 0.0109 mol), PPh_3Br_2 (4.61 g, 0.0109 mol), and NET_3 (4 mL, 0.0287 mol) in 10 mL of toluene. A 2:1 heptane:toluene solution was added to the oily residue to afford 3.81 g of the desired product (79%). $^1\text{H NMR}$ (300 MHz, C_6D_6): $\delta = 3.53$ (s, 6H, *m*- OCH_3), 3.61 (s, 3H, *p*- OCH_3), 5.92 (s, 2H, *Ar-H*), 7.45–7.60 (overlapping peaks, 9H, phosphine *o*- and *p*-*Ar-H*), 7.70–7.80 (m, 6H, *Ar-H*). **3b** was prepared similarly to **3a** with 3.8 g of iminophosphorane, 330 mg of glyoxal trimer, and 1 g of 4 \AA molecular sieves in refluxing THF overnight. A substantial amount of iminophosphorane was recovered, and 300 mg of product was isolated (20%). The ligands isolated contained 5% phosphine-containing complex. $^1\text{H NMR}$ (300 MHz, CD_2Cl_2): $\delta = 3.80$ (s, 6H, *p*- OCH_3), 3.87 (s, 12H, *m*- OCH_3), 6.604 (s, 4H, *Ar-H*), 8.40 (s, 2H, $\text{N}=\text{C}-\text{H}$). ESMS, Calcd for $\text{C}_{20}\text{H}_{24}\text{N}_2\text{O}_6\text{H}$ ($[\text{M} + \text{H}]^+$): 389.1713. Found: 389.1723.

1,4-Bis(3-methoxy-5-(trifluoromethyl)phenyl)-1,4-diaza-1,3-butadiene ($^{\text{OMeCF}_3\text{Ar}}\text{DAB}^{\text{H}}$, **3c**). The iminophosphorane was synthesized similarly starting with 3-methoxy-5-trifluoromethyl-aniline (1.25 g, 0.00654 mol), PPh_3Br_2 (2.76 g, 0.00654 mol), and NET_3 (2 mL, 0.0143 mol). After removing NET_3HBr and solvent, 100 mL of 4:1 petroleum ether:toluene mixture was added to the oily residue to yield 2.25 g (70% after correcting for toluene content) of light tan solid. The product contains ~ 8 wt % toluene. $^1\text{H NMR}$ (300 MHz, C_6D_6): $\delta = 3.18$ (s,

3H, OCH_3), 6.69 (br s, 1H), 6.84 (br s, 1H), 6.9–7.2 (overlapping peaks, 9H, phosphine *o,p*-*Ar-H*), 7.22 (br s, 1H, *Ar-H*), 7.70 (ddd, 6H, $J = 1.5$ Hz, 7.5 Hz, 12 Hz, phosphine *m*-*Ar-H*). Iminophosphorane (1.16 g, 2.56 mmol), glyoxal trimer (90 mg, 0.428 mmol), and 2 g of activated molecular sieves were added to a reaction flask containing dry THF. The mixture was heated at $\sim 80^\circ\text{C}$ overnight. After 17 h, examination of an aliquot of the mixture indicated little progress in reaction. Another 100 mg of glyoxal trimer was added to the mixture, the reaction flask was closed off, and the reaction temperature was raised to $\sim 100^\circ\text{C}$. After 14 h, the reaction mixture was cooled, and another aliquot of the mixture was taken. The conversion was $\sim 57\%$, but the $^1\text{H NMR}$ also indicated the existence of a third species ($\sim 5\%$ of the total product) besides the starting iminophosphorane and the diimine. Since it was not clear whether this species was merely a side-product or the decomposition product of the diimine, the reaction mixture was worked up immediately, and 200 mg of yellow solids was collected (38.5%, contains $\sim 5\%$ starting iminophosphoranes). $^1\text{H NMR}$ (300 MHz, C_6D_6): $\delta = 3.06$ (s, 6H, OCH_3), 6.76 (br s, 2H, *Ar-H*), 6.98 (br s, 2H, *Ar-H*), 7.09 (br s, 2H, *Ar-H*), 7.99 (s, 2H, $\text{N}=\text{C}-\text{H}$). ESMS, Calcd for $\text{C}_{18}\text{H}_{14}\text{N}_2\text{O}_2\text{F}_6\text{H}$ ($[\text{M} + \text{H}]^+$): 405.1038. Found: 405.1051.

($^{\text{tBu}_2\text{OMeAr}}\text{DAB}^{\text{Me}}\text{PtMe}_2$) **1a** (200 mg, 0.384 mmol) and bis(dimethyl(μ -dimethyl sulfide)platinum(II)) (109.9 mg, 0.191 mmol) were added to a receiving flask equipped with a 180° valve. The flask was cooled to -78°C and evacuated, and 10 mL of toluene was vacuum transferred onto the solids. The dry ice bath was then removed, and the reaction mixture was allowed to warm gradually to room temperature and was left stirring at room temperature for 3 nights (NB: The reaction was probably done after 10 h). The solution turned quickly from pale yellow to deep purple upon warming to room temperature. At the end of the reaction, there was a considerable amount of purple solid suspended in the purple solution. Toluene was removed in vacuo, and 15 mL of petroleum ether was added to the purple solid residues. The insolubles were collected, washed with petroleum ether (4×5 mL), and dried over an aspirator for several hours. **4a** was collected as a purple-red solid (265 mg, 92.5%). $^1\text{H NMR}$ (500 MHz, CD_2Cl_2): $\delta = 0.93$ (s, 6H, $^2J_{\text{Pt-H}} = 86.7$ Hz, $\text{Pt}-\text{CH}_3$), 1.452 (s, 36H, $\text{C}(\text{CH}_3)_3$), 1.48 (s, 6H, $\text{N}=\text{C}-\text{CH}_3$), 3.73 (s, 6H, OCH_3), 6.865 (s, 4H, *Ar-H*). ^{13}C $\{^1\text{H}\}$ NMR (125 MHz, CD_2Cl_2): $\delta = -13.21$ ($^1J_{\text{Pt-C}} = 789$ Hz, $\text{Pt}-\text{CH}_3$), 21.30 ($\text{N}=\text{C}-\text{CH}_3$), 32.37 ($\text{C}(\text{CH}_3)_3$), 36.45 ($\text{C}(\text{CH}_3)_3$), 64.91 (OCH_3), 120.68 (*o*-*Ar-C*), 142.96, 144.46, 157.87 (*Ar-C*), 171.08 ($\text{N}=\text{C}-\text{CH}_3$). The compound slowly decomposes in methylene chloride. ESMS, Calcd for $\text{C}_{35}\text{H}_{55}\text{N}_2\text{O}_2\text{PtCH}_3\text{CN}$ ($[\text{M} - \text{Me} + \text{NCMe}]^+$): 770.4156 (^{194}Pt), 771.4180 (^{195}Pt), 772.4192 (^{196}Pt). Found: 770.4173, 771.4180, 772.4189. Anal. Calcd for $\text{C}_{36}\text{H}_{58}\text{N}_2\text{O}_2\text{Pt}$: C, 59.97; H, 7.84; N, 3.76. Found: C, 52.2/53.53; H, 7.00/7.24; N, 3.33/3.34.

($^{\text{tBu}_2\text{Ar}}\text{DAB}^{\text{Me}}\text{PtMe}_2$) **4b** was synthesized similarly from **1b** (160 mg, 0.348 mmol) and bis(dimethyl(μ -dimethyl sulfide)platinum(II)) (100 mg, 0.174 mmol). **4b** was collected as a purple-red solid (220 mg, 92%). $^1\text{H NMR}$ (500 MHz, CD_2Cl_2): $\delta = 0.90$ (s, 6H, $^2J_{\text{Pt-H}} = 85.3$ Hz, $\text{Pt}-\text{CH}_3$), 1.36 (s, 36H, $\text{C}(\text{CH}_3)_3$), 1.48 (s, 6H, $\text{N}=\text{C}-\text{CH}_3$), 6.83 (d, $^3J_{\text{H-H}} = 1.5$ Hz, 4H, *o*-*Ar-H*), 7.32 (t, $^3J_{\text{H-H}} = 1.5$ Hz, 4H, *p*-*Ar-H*). ^{13}C $\{^1\text{H}\}$ NMR (125 MHz, CD_2Cl_2): $\delta = -13.13$ ($\text{Pt}-\text{CH}_3$), 21.24 ($\text{N}=\text{C}-\text{CH}_3$), 31.69 ($\text{C}(\text{CH}_3)_3$), 35.49 ($\text{C}(\text{CH}_3)_3$), 116.76 (*o*-*Ar-C*), 120.18 (*p*-*Ar-C*), 147.68, 151.98 (*Ar-C*), 171.03 ($\text{N}=\text{C}-\text{CH}_3$). The compound slowly decomposes in methylene chloride. ESMS, Calcd for $\text{C}_{33}\text{H}_{51}\text{N}_2\text{PtCH}_3\text{CN}$ ($[\text{M} - \text{Me} + \text{NCMe}]^+$): 710.3945 (^{194}Pt), 711.3969 (^{195}Pt), 712.3980 (^{196}Pt). Found: 710.3945, 711.3951, 712.3969. Anal. Calcd for $\text{C}_{34}\text{H}_{54}\text{N}_2\text{Pt}$: C, 59.54; H, 7.94; N, 4.08. Found: C, 58.29/58.95; H, 7.76/7.86; N, 4.07/4.01.

($^{\text{OMe}_3\text{Ar}}\text{DAB}^{\text{Me}}\text{PtMe}_2$) **4c** was synthesized similarly from **1c** (200 mg, 0.48 mmol) and bis(dimethyl(μ -dimethyl sulfide)platinum(II)) (138 mg, 0.24 mmol). **4c** was collected as a purple-red solid (278 mg, 90%). $^1\text{H NMR}$ (500 MHz, CD_2Cl_2): $\delta = 1.05$ (s, 6H, $^2J_{\text{Pt-H}} = 85.2$ Hz, $\text{Pt}-\text{CH}_3$), 1.48 (s, 6H, $\text{N}=\text{C}-\text{CH}_3$), 3.82 (s, 6H, OCH_3), 3.84 (s, 12H, OCH_3), 6.24 (s, 4H, *Ar-H*). ^{13}C $\{^1\text{H}\}$ NMR (125 MHz, CD_2Cl_2): $\delta = -13.29$ ($^1J_{\text{Pt-C}} = 798$ Hz, $\text{Pt}-\text{CH}_3$), 21.40 ($\text{N}=\text{C}-\text{CH}_3$),

56.72 (OCH₃), 61.17 (OCH₃), 99.77 (*o*-Ar-C), 136.46, 144.12, 154.02 (Ar-C), 171.67 (N=C-CH₃). The compound slowly decomposes in methylene chloride. ESMS, Calcd for C₂₃H₃₁N₂O₆PtCH₃CN ([M - Me + NCMe]⁺): 666.2075 (¹⁹⁴Pt), 667.2098 (¹⁹⁵Pt), 668.2107 (¹⁹⁶Pt). Found: 666.2085, (¹⁹⁴Pt), 667.2090, 668.2101. Anal. Calcd for C₂₄H₃₄N₂O₆Pt: C, 44.93; H, 5.34; N, 4.37. Found: C, 44.02; H, 5.22; N, 4.16.

(^{OMeCF₃Ar}DAB^{Me})PtMe₂ (**4d**). **4d** was synthesized similarly from **1d** (100 mg, 0.23 mmol) and bis(dimethyl(*μ*-dimethyl sulfide)platinum(II)) (66.5 mg, 0.116 mmol). **4d** was collected as a purple-red solid (130 mg, 85.4%). ¹H NMR (500 MHz, CD₂Cl₂): δ = 1.07 (s, 6H, ²J_{Pt-H} = 87.2 Hz, Pt-CH₃), 1.41 (s, 6H, N=C-CH₃), 3.900 (s, 6H, OCH₃), 6.78 (m, 2H, Ar-H), 6.89 (m, 2H, Ar-H), 7.10 (m, 2H, Ar-H). ¹³C {¹H} NMR (125 MHz, CD₂Cl₂): δ = -12.91 (Pt-CH₃), 21.60 (N=C-CH₃), 56.51 (OCH₃), 109.58 (³J_{C-F} = 3 Hz, Ar-C), 111.36 (³J_{C-F} = 3 Hz, Ar-C), 111.55, 124.30 (¹J_{C-F} = 275 Hz, CF₃), 132.64 (²J_{C-F} = 32.7 Hz, CF₃-C), 149.74, 161.01 (Ar-C), 171.869 (N=C-CH₃). ¹⁹F NMR (C6D6): δ = -63.70. The compound slowly decomposes in methylene chloride. ESMS, Calcd for C₂₁H₂₁N₂O₂F₆PtCH₃CN ([M - Me + NCMe]⁺): 682.1400 (¹⁹⁴Pt), 683.1423 (¹⁹⁵Pt), 684.1431 (¹⁹⁶Pt). Found: 682.1382, 683.1411, 684.1393. Anal. Calcd for C₂₂H₂₄N₂O₂F₆Pt: C, 40.19; H, 3.68; N, 4.26. Found: C, 38.65/38.88; H, 3.53/3.53; N, 3.95/4.04.

(^{Me₃Ar}DAB^{Me})PtMe₂ (**5a**). **5a** was synthesized similarly from **2a** (111.6 mg, 0.348 mmol) and bis(dimethyl(*μ*-dimethyl sulfide)platinum(II)) (100 mg, 0.174 mmol). **5a** was collected as a purple-red solid (160 mg, 84%). ¹H NMR (500 MHz, CD₂Cl₂): δ = 0.79 (s, 6H, ²J_{Pt-H} = 85.7 Hz, Pt-CH₃), 1.24 (s, 6H, N=C-CH₃), 2.11 (s, 12H, *o*-CH₃), 2.37 (s, 6H, *p*-CH₃), 7.01 (s, 4H, Ar-H). ¹³C {¹H} NMR (125 MHz, CD₂Cl₂): δ = -14.92 (¹J_{Pt-C} = 797 Hz, Pt-CH₃), 17.48 (*o*-CH₃), 20.18 (N=C-CH₃), 21.14 (*p*-CH₃), 128.84 (*m*-Ar-C), 128.87 (*o*-Ar-C), 135.77 (*p*-Ar-C), 143.77 (*ipso*-Ar-C), 170.79 (N=C-CH₃). The compound slowly decomposes in methylene chloride. ESMS, Calcd for C₂₃H₃₁N₂PtCH₃CN ([M - Me + NCMe]⁺): 570.2380 (¹⁹⁴Pt), 571.2403 (¹⁹⁵Pt), 572.2412 (¹⁹⁶Pt). Found: 570.2391, 571.2369, 572.2413. Anal. Calcd for C₂₄H₃₄N₂Pt: C, 52.83; H, 6.28; N, 5.13. Found: C, 40.75/50.99; H, 4.79/6.17; N, 3.89/4.88.

(^{Me₂BrAr}DAB^{Me})PtMe₂ (**5c**). **5c** was synthesized similarly from **2c** (78.4 mg, 0.174 mmol) and bis(dimethyl(*μ*-dimethyl sulfide)platinum(II)) (50 mg, 0.087 mmol). **5c** was collected as a purple-red solid (100 mg, 85%). ¹H NMR (500 MHz, CD₂Cl₂): δ = 0.89 (s, 6H, ²J_{Pt-H} = 86 Hz, Pt-CH₃), 1.20 (s, 6H, N=C-CH₃), 2.13 (s, 12H, *o*-CH₃), 7.37 (s, 4H, Ar-H). ¹³C {¹H} NMR (125 MHz, CD₂Cl₂): δ = -14.46 (¹J_{Pt-C} = 800 Hz, Pt-CH₃), 17.44 (*o*-CH₃), 20.45 (N=C-CH₃), 119.21 (Br-Ar-C), 131.01 (*m*-Ar-C), 131.55 (*o*-Ar-C), 145.23 (*ipso*-Ar-C), 170.96 (N=C-CH₃). The compound slowly decomposes in methylene chloride. ESMS, Calcd for C₂₁H₂₅N₂Br₂PtCH₃CN ([M - Me + NCMe]⁺): 699.0300 (⁷⁹Br⁸¹Br¹⁹⁵Pt), 700.0275 (⁷⁹Br⁸¹Br¹⁹⁴Pt), 702.0276 (⁸¹Br⁸¹Br¹⁹⁴Pt), 703.0278 (⁸¹Br⁸¹Br¹⁹⁵Pt), 704.0283 (⁸¹Br⁸¹Br¹⁹⁶Pt). Found: 699.0306, 700.0275, 702.0278, 703.0297, 704.0309. Anal. Calcd for C₂₂H₂₈N₂Br₂Pt: C, 39.13; H, 4.18; N, 4.15. Found: C, 38.24/38.03; H, 4.07/4.01; N, 3.93/3.88.

(^{tBu₂Ar}DAB^H)PtMe₂ (**6a**). **6a** was synthesized similarly from **3a** (150 mg, 0.347 mmol) and bis(dimethyl(*μ*-dimethyl sulfide)platinum(II)) (100 mg, 0.174 mmol). **6a** was collected as a dark green/tan black solid (187 mg, 82%). ¹H NMR (500 MHz, CD₂Cl₂): δ = 1.39 (s, 36H, C(CH₃)₃), 1.65 (s, 6H, ²J_{Pt-H} = 85.4 Hz, Pt-CH₃), 7.27 (d, ³J_{H-H} = 1.5 Hz, 4H, *o*-Ar-H), 7.50 (t, ³J_{H-H} = 1.5 Hz, 4H, *p*-Ar-H), 9.41 (s, 2H, ³J_{Pt-H} = 24.1 Hz). ¹³C {¹H} NMR (125 MHz, CD₂Cl₂): δ = -11.12 (Pt-CH₃), 31.69 (C(CH₃)₃), 35.53 (C(CH₃)₃), 118.12 (*o*-Ar-C), 122.90 (*p*-Ar-C), 149.91 (*ipso*-Ar-C), 152.30 (*m*-Ar-C), 161.87 (N=C-H). ESMS, Calcd for C₃₁H₄₇N₂PtCH₃CN ([M - Me + NCMe]⁺): 682.3632 (¹⁹⁴Pt), 683.3655 (¹⁹⁵Pt), 684.3666 (¹⁹⁶Pt). Found: 682.3641, 683.3646, 684.3667. Anal. Calcd for C₃₂H₅₀N₂Pt: C, 58.43; H, 7.66; N, 4.26. Found: C, 56.16/56.16; H, 7.85/7.37; N, 3.99/4.00.

(^{OMe₃Ar^H}DAB)PtMe₂ (**6b**). **6b** was synthesized similarly from **3b** (95 mg, 0.245 mmol) and bis(dimethyl(*μ*-dimethyl sulfide)platinum(II)) (70 mg, 0.122 mmol). The petroleum ether insolubles were collected, washed with benzene/methylene chloride (to remove triphenylphosphine oxide contained in **3b**), diethyl ether (20 mL), and petroleum ether (4 × 20 mL), and dried over an aspirator for several hours. **6b** was collected as a dark green/tan solid (100 mg, 67%). ¹H NMR (500 MHz, CD₂Cl₂): δ = 1.88 (s, 6H, ²J_{Pt-H} = 86 Hz, Pt-CH₃), 3.96 (s, 6H, *p*-OCH₃), 4.01 (s, 12H, *m*-OCH₃), 6.82 (s, 4H, Ar-H), 9.52 (s, 2H, ³J_{Pt-H} = 27 Hz). ¹³C {¹H} NMR (125 MHz, CD₂Cl₂): δ = -11.41 (Pt-CH₃), 54.07 (*m*-OCH₃), 56.45 (*p*-OCH₃), 101.08(*o*-Ar-C), 128.51 (*p*-Ar-C), 145.80 (*ipso*-Ar-C), 153.62 (*m*-Ar-C), 161.21 (N=C-H). ESMS, Calcd for C₂₁H₂₇N₂O₆PtCH₃CN ([M - Me + NCMe]⁺): 638.1761 (¹⁹⁴Pt), 639.1785 (¹⁹⁵Pt), 640.1793 (¹⁹⁶Pt). Found: 638.1774, 639.1793, 640.1801.

(^{OMeCF₃Ar}DAB^H)PtMe₂ (**6c**). **3c** (80 mg, 0.198 mmol) and bis(dimethyl(*μ*-dimethyl sulfide)platinum(II)) (containing some (SMe₂)₂-PtMe₂ monomer, 61 mg, ~0.1 mmol) were added to a reaction flask equipped with a 180° valve. Methylene chloride (5 mL) was added to the mixture in air. The solution turned quickly from pale yellow to green. The volatiles were partially removed after one-half an hour at -20 °C to remove SMe₂. The flask was then back-filled with Ar, and 2 mL more of methylene chloride was added to the reaction mixture. The mixture was then stirred at room temperature for another one-half an hour to an hour. The solvent was then removed at -20 °C. Methylene chloride (0.5 mL) and petroleum ether (5 mL) were added to the dark solid residue, and the insolubles were collected and washed with petroleum ether (3 × 2 mL). **6c**, the dark green/black solid, was dried over an aspirator for 2 h (104 mg, 84%). NB: This reaction did not work in toluene; the green color initially formed faded after 4 h at room temperature, and an intractable mixture was left behind. ¹H NMR (500 MHz, CD₂Cl₂): δ = 1.91 (s, 6H, ²J_{Pt-H} = 87 Hz, Pt-CH₃), 3.94 (s, 6H, OCH₃), 7.21 (s, 2H, Ar-H), 7.24 (s, 2H, Ar-H), 7.26 (s, 2H, Ar-H), 9.64 (s, 2H, ³J_{Pt-H} = 27 Hz). ¹³C {¹H} NMR (125 MHz, CD₂Cl₂): δ = -11.00 (Pt-CH₃), 56.27 (OCH₃), 111.36 (³J_{C-F} = 3.8 Hz, Ar-C), 112.11 (³J_{C-F} = 3.6 Hz, Ar-C), 112.42, 123.81 (¹J_{C-F} = 272 Hz, CF₃), 132.49 (²J_{C-F} = 33.5 Hz, CF₃-C), 151.58, 160.57 (Ar-C), 162.52 (N=C-H). ESMS, Calcd for C₁₉H₁₇N₂O₂F₆PtCH₃CN ([M - Me + NCMe]⁺): 654.1086 (¹⁹⁴Pt), 655.1110 (¹⁹⁵Pt), 656.1118 (¹⁹⁶Pt). Found: 654.1078, 655.1118, 656.1111.

(^{tBu₂OMeAr}DAB^{Me})PtMe(CO)]⁺[BF₄]⁻ (**7a**). To a suspension of **4a** (11.4 mg, 0.015 mmol) in ~2 mL of trifluoroethanol (TFE) was added an aqueous solution of HBF₄ (2 μL, 0.015 mmol). After stirring at room temperature for a few minutes, a homogeneous orange solution was obtained. The reaction flask was degassed and backfilled with 1 atm of CO. The color of the solution changed to bright yellow almost instantaneously. The mixture was stirred under 1 atm of CO for 24 h. TFE was then removed at -20 to 0 °C in vacuo, and a small amount of petroleum ether was added to the oily residue to effect solidification (scratching the reaction flask helps). PE was then removed on the vacuum line, and the resulting yellow solid (7 mg, 54%) was dried for 30 min. The product contained a small amount of TFE, which was hard to remove. ¹H NMR (300 MHz, CD₂Cl₂): δ = 0.72 (s, 3H, ²J_{Pt-H} = 66 Hz, Pt-CH₃), 1.45, 1.46 (s, 18H each, C(CH₃)₃), 2.36, 2.44 (s, 3H each, N=C-CH₃), 3.73, 3.73 (s, 3H each, OCH₃), 6.95, 7.18 (s, 2H each, Ar-H). ¹³C {¹H} NMR (75 MHz, CD₂Cl₂): δ = -10.45 (Pt-CH₃), 20.63, 22.32 (N=C-CH₃), 31.90, 31.96 (C(CH₃)₃), 36.48, 36.52 (C(CH₃)₃), 64.91, 64.99 (OCH₃), 119.90, 120.40, 137.49, 142.12, 145.82, 146.04, 159.17, 159.88 (Ar-C), 155.52, 175.98, 189.08. IR (CH₂Cl₂): ν(CO) = 2103.5 cm⁻¹. The compound decomposes in methylene chloride. Anal. Calcd for C₃₆H₅₅N₂O₃PtBF₄: C, 51.13; H, 6.56. Found: C, 42.25; H, 5.27.

(^{tBu₂Ar}DAB^{Me})PtMe(CO)]⁺[BF₄]⁻ (**7b**). **7b** was synthesized similarly from **4b** (15.7 mg, 0.023 mmol) and an aqueous solution of HBF₄ (3 μL, 0.023 mmol) in 3 mL of TFE. The yellow product contained a small amount of TFE, which was hard to remove. ¹H NMR (300 MHz,

CD_2Cl_2): $\delta = 0.69$ (s, 3H, ${}^2J_{\text{Pt-H}} = 69$ Hz, Pt-CH₃), 1.36, 1.37 (s, 18H each, C(CH₃)₃), 2.35, 2.45 (s, 3H each, N=C-CH₃), 6.91 (d, ${}^4J_{\text{H-H}} = 1.8$ Hz, 2H, Ar-H), 7.13 (d, ${}^4J_{\text{H-H}} = 1.8$ Hz, 2H, Ar-H), 7.45, 7.46 (overlapping t, 2H total, Ar-H). ${}^{13}\text{C}$ { ${}^1\text{H}$ } NMR (75 MHz, CD_2Cl_2): $\delta = -10.42$ (Pt-CH₃), 20.57, 22.34 (N=C-CH₃), 31.32 (overlapping C(CH₃)₃), 35.48, 35.54 (C(CH₃)₃), 115.49, 116.32, 122.37, 123.0, 153.15, 153.40 (Ar-C), 189.16. Resonances for two Ar-C and N=C-CH₃ were not located. IR (CH_2Cl_2): $\nu(\text{CO}) = 2104.6$ cm^{-1} . The compound decomposes in methylene chloride. Anal. Calcd for C₃₄H₅₁N₂PtBF₄: C, 51.98; H, 6.54; N, 3.57. Found: C, 49.04/48.84; H, 6.18/6.21; N, 3.35/3.32.

$[(\text{OMe}_3\text{Ar}^{\text{DABMe}})\text{PtMe}(\text{CO})]^+[\text{BF}_4]^-$ (**7c**). **7c** was synthesized similarly from **4c** (14.7 mg, 0.023 mmol) and an aqueous solution of HBF₄ (3 μL , 0.023 mmol) in 3 mL of TFE. 13 mg of orange powder was obtained (80%). The product contained a small amount of TFE, which was hard to remove. ${}^1\text{H}$ NMR (300 MHz, CD_2Cl_2): $\delta = 0.84$ (s, 3H, ${}^2J_{\text{Pt-H}} = 66$ Hz, Pt-CH₃), 2.34, 2.47 (s, 3H each, N=C-CH₃), 3.82, 3.86, 3.88 (s, 6H each, OCH₃), 6.37, 6.54 (s, 2H each, Ar-H). ${}^{13}\text{C}$ { ${}^1\text{H}$ } NMR (75 MHz, CD_2Cl_2): $\delta = -10.35$ (Pt-CH₃), 20.66 (overlapping N=C-CH₃), 56.56, 56.86, 61.10, 61.20 (OCH₃), 98.25, 98.64, 99.42, 99.75, 138.41, 143.02, 154.31, 154.42 (Ar-C), 163.53, 177.29, 191.04. IR (CH_2Cl_2): $\nu(\text{CO}) = 2105.8$ cm^{-1} . The compound slowly decomposes in methylene chloride. Anal. Calcd for C₂₄H₃₁N₂O₇PtBF₄: C, 38.88; H, 4.21; N, 3.78. Found: C, 36.64/36.70; H, 4.00/3.99; N, 3.34/3.26.

$[(\text{OMeCF}_3\text{Ar}^{\text{DABMe}})\text{PtMe}(\text{CO})]^+[\text{BF}_4]^-$ (**7d**). **7d** was synthesized similarly from **4d** (15.1 mg, 0.023 mmol) and an aqueous solution of HBF₄ (3 μL , 0.023 mmol) in 3 mL of TFE. 10 mg of yellow/orange powder was collected (62%). The product contained a small amount of TFE, which was hard to remove. ${}^1\text{H}$ NMR (300 MHz, CD_2Cl_2): $\delta = 0.77$ (s, 3H, ${}^2J_{\text{Pt-H}} = 68$ Hz, Pt-CH₃), 2.33, 2.47 (s, 3H each, N=C-CH₃), 3.93, 3.92 (s, 3H each, OCH₃), 6.93, 7.09, 7.20, 7.22 (overlapping broad m, 6H total, Ar-H). ${}^1\text{H}$ NMR (300 MHz, TFE-*d*₃): $\delta = 0.83$ (s, 3H, ${}^2J_{\text{Pt-H}} = 66$ Hz, Pt-CH₃), 2.27, 2.42 (s, 3H each, N=C-CH₃), 3.90, 3.91 (s, 6H total, OCH₃), 6.82, 6.91, 6.97, 7.08 (broad s, 1H each, Ar-H), 7.27, 7.29 (broad s, 2H total, Ar-H). ${}^{13}\text{C}$ { ${}^1\text{H}$ } NMR (75 MHz, TFE-*d*₃): $\delta = -10.50$ (Pt-CH₃), 20.68, 22.56 (N=C-CH₃), 56.92, 56.95 (OCH₃), 110.68 (q, ${}^3J_{\text{C-F}} \approx 3$ Hz, *o*-Ar-C), 111.18 (*o*-Ar-C), 112.01 (q, ${}^3J_{\text{C-F}} \approx 3$ Hz, *o*-Ar-C), 112.68 (*o*-Ar-C), 113.15 (overlapping q, ${}^3J_{\text{C-F}} \approx 3$ Hz, *p*-Ar-C), 135.90 (q, ${}^2J_{\text{C-F}} \approx 23$ Hz, C-CF₃), 136.35 (q, ${}^2J_{\text{C-F}} \approx 23$ Hz, C-CF₃), 145.15, 149.641, 163.11, 163.30 (Ar-C), 179.03, 191.28. Unable to find CF₃ resonances, which are probably buried under CF₃CD₂OD resonances. IR (CH_2Cl_2): $\nu(\text{CO}) = 2110.1$ cm^{-1} . The compound decomposes quickly in methylene chloride and slowly in the solid state.

$[(\text{CF}_3\text{Ar}^{\text{DABMe}})\text{PtMe}(\text{CO})]^+[\text{BF}_4]^-$ (**7e**). **7e** was synthesized similarly from **4e** (11.2 mg, 0.015 mmol) and an aqueous solution of HBF₄ (2 μL , 0.015 mmol) in 2 mL of TFE. The product contained a significant amount of TFE, which was hard to remove. ${}^1\text{H}$ NMR (300 MHz, TFE-*d*₃): $\delta = 0.77$ (s, 3H, ${}^2J_{\text{Pt-H}} = 66$ Hz, Pt-CH₃), 2.31, 2.45 (s, 3H each, N=C-CH₃), the peaks were completely deuterated within an hour at room temperature), 7.65 (d, ${}^4J_{\text{H-H}} = 1.5$ Hz, 2H, *o*-Ar-H), 7.80 (d, ${}^4J_{\text{H-H}} = 1.5$ Hz, 2H, *o*-Ar-H), 8.05 (t, ${}^4J_{\text{H-H}} = 1.5$ Hz, 1H, *p*-Ar-H), 8.08 (t, ${}^4J_{\text{H-H}} = 1.5$ Hz, 1H, *p*-Ar-H). ${}^{13}\text{C}$ { ${}^1\text{H}$ } NMR (75 MHz, TFE-*d*₃): $\delta = -10.09$ (Pt-CH₃), 123.01 (q, ${}^3J_{\text{C-F}} \approx 3$ Hz), 124.86 (q, ${}^3J_{\text{C-F}} \approx 3$ Hz), 127.6 (q, ${}^1J_{\text{C-F}} \approx 273$ Hz), 135.84 (q, ${}^2J_{\text{C-F}} \approx 21$ Hz, C-CF₃), 136.30 (q, ${}^2J_{\text{C-F}} \approx 3$ Hz, C-CF₃), 144.67, 148.99 (Ar-C), 180.43, 192.41. Unable to find one set of CF₃ resonances and several Ar-C resonances, which are probably buried under CF₃CD₂OD resonances; unable to find resonances corresponding to diimine methyl backbone, which were completely deuterated within an hour at room temperature in TFE-*d*₃. This significantly reduces the intensity of the ${}^{13}\text{C}$ signals. IR (CH_2Cl_2): $\nu(\text{CO}) = 2113.5$ cm^{-1} . The compound decomposes quickly in methylene chloride and in the solid state.

$[(\text{C}^{\text{Me}_2}\text{Ar}^{\text{DABMe}})\text{PtMe}(\text{CO})]^+[\text{BF}_4]^-$ (**7f**). **7f** was synthesized similarly from **4f** (19.8 mg, 0.038 mmol) and an aqueous solution of HBF₄

(5 μL , 0.038 mmol) in 8 mL of TFE. 10 mg of brown solid was obtained (43%). The product contained a small amount of TFE, which was hard to remove. ${}^1\text{H}$ NMR (300 MHz, CD_2Cl_2): $\delta = 0.72$ (s, 3H, ${}^2J_{\text{Pt-H}} = 68$ Hz, Pt-CH₃), 2.30, 2.42 (s, 3H each, N=C-CH₃), 2.38 (s, 12H, *m*-CH₃), 6.70 (br, 2H, *m*-Ar-H), 6.89 (br, 2H, *o*-Ar-H), 7.04 (br, 1H, *p*-Ar-H), 7.06 (br, 1H, *p*-Ar-H). IR (CH_2Cl_2): $\nu(\text{CO}) = 2105.7$ cm^{-1} .

$[(\text{Me}_3\text{Ar}^{\text{DABMe}})\text{PtMe}(\text{CO})]^+[\text{BF}_4]^-$ (**8a**). **8a** was synthesized similarly from **5a** (16.7 mg, 0.031 mmol) and an aqueous solution of HBF₄ (4 μL , 0.031 mmol) in 5 mL of TFE. 7 mg of yellow powder was obtained (35%). The product contained a small amount of TFE, which was hard to remove. ${}^1\text{H}$ NMR (300 MHz, CD_2Cl_2): $\delta = 0.58$ (s, 3H, ${}^2J_{\text{Pt-H}} = 66$ Hz, Pt-CH₃), 2.16, 2.31 (s, 6H each, *o*-Ar-CH₃), 2.21, 2.41 (s, 3H each, N=C-CH₃), 2.36 (overlapping s, 6H total, *p*-Ar-CH₃), 7.06, 7.07 (s, 4H total, Ar-H). ${}^{13}\text{C}$ { ${}^1\text{H}$ } NMR (75 MHz, CD_2Cl_2): $\delta = -10.40$ (Pt-CH₃), 18.04, 18.07 (*o*-Ar-CH₃), 19.84, 21.22, 21.28, 21.45 (*p*-Ar-C and N=C-CH₃), 127.72, 129.61, 129.85, 129.96, 137.63, 138.77, 139.28, 143.23 (Ar-C), 179.25, 191.39. IR (CH_2Cl_2): $\nu(\text{CO}) = 2108.3$ cm^{-1} . The compound decomposes in methylene chloride, giving methane and Pt black. Anal. Calcd for C₂₄H₃₁N₂O₇PtBF₄: C, 44.66; H, 4.84; N, 4.34. Found: C, 34.36/34.14; H, 3.74/3.67; N, 3.08/3.12. The sample appeared to contain silica from the frit; although the C:H:N are all low, they are in the correct ratio.

$[(\text{Me}_2\text{Ar}^{\text{DABMe}})\text{PtMe}(\text{CO})]^+[\text{BF}_4]^-$ (**8b**). **8b** was synthesized similarly from **5b** (19.8 mg, 0.038 mmol) and an aqueous solution of HBF₄ (5 μL , 0.038 mmol) in 5 mL of TFE. 16 mg of yellow powder was obtained (76%). The product contained a small amount of TFE, which was hard to remove. ${}^1\text{H}$ NMR (300 MHz, CD_2Cl_2): $\delta = 0.57$ (s, 3H, ${}^2J_{\text{Pt-H}} = 66$ Hz, Pt-CH₃), 2.22, 2.37 (s, 6H each, *o*-Ar-CH₃), 2.24, 2.44 (s, 3H each, N=C-CH₃), 7.20-7.40 (m, 6H total, Ar-H). ${}^{13}\text{C}$ { ${}^1\text{H}$ } NMR (75 MHz, CD_2Cl_2): $\delta = -10.55$ (Pt-CH₃), 18.12, 18.17 (*o*-Ar-CH₃), 19.88, 21.49 (N=C-CH₃), 128.09, 128.79, 129.27, 129.30, 129.44, 130.00, 140.42, 145.78 (Ar-C), 162.69, 179.25, 190.39. IR (CH_2Cl_2): $\nu(\text{CO}) = 2109.6$ cm^{-1} . ESMS, Calcd for C₂₂H₂₇N₂O₇Pt ([M]⁺): 529.1750 (¹⁹⁴Pt), 530.1774 (¹⁹⁵Pt), 531.1782 (¹⁹⁶Pt). Found: 529.1764, 530.1771, 531.1781. Anal. Calcd for C₂₂H₂₇N₂O₇PtBF₄: C, 42.80; H, 4.41; N, 4.54. Found: C, 41.17/40.94; H, 4.44/4.19; N, 4.18/4.16. The compound decomposes in methylene chloride.

$[(\text{Me}_2\text{Br}^{\text{Ar}})\text{PtMe}(\text{CO})]^+[\text{BF}_4]^-$ (**8c**). **8c** was synthesized similarly from **5c** (25.8 mg, 0.038 mmol) and an aqueous solution of HBF₄ (5 μL , 0.038 mmol) in 5 mL of TFE. 16 mg of yellow powder was obtained (60%). The product contained a small amount of TFE, which was hard to remove. ${}^1\text{H}$ NMR (300 MHz, CD_2Cl_2): $\delta = 0.61$ (s, 3H, ${}^2J_{\text{Pt-H}} = 69$ Hz, Pt-CH₃), 2.20, 2.35 (s, 6H each, Ar-CH₃), 2.25, 2.45 (s, 3H each, N=C-CH₃), 7.43, 7.44 (s, 2H each, Ar-H). ${}^{13}\text{C}$ { ${}^1\text{H}$ } NMR (75 MHz, CD_2Cl_2): $\delta = -10.22$ (Pt-CH₃), 18.03, 18.07 (Ar-CH₃), 20.12, 21.73 (overlapping N=C-CH₃), 122.09, 122.66, 130.59, 132.08, 132.13, 132.19, 132.27, 132.41 (Ar-C), 179.91, 191.04. IR (CH_2Cl_2): $\nu(\text{CO}) = 2111.6$ cm^{-1} . The compound slowly decomposes in methylene chloride. ESMS, Calcd for C₂₂H₂₅N₂Br₂O₇Pt ([M]⁺): 684.9958 (⁷⁹Br-⁷⁹Br-¹⁹⁴Pt), 685.9984 (⁷⁹Br-⁷⁹Br-¹⁹⁵Pt), 686.9958, 687.9968, 688.9960, 689.9961 (⁸¹Br-⁸¹Br-¹⁹⁵Pt), 690.9966 (⁷⁹Br-⁷⁹Br-¹⁹⁵Pt). Found: 684.9980, 685.9995, 686.9962, 687.9972, 688.9959, 690.0007, 690.9974. Anal. Calcd for C₂₂H₂₅Br₂N₂O₇PtBF₄: C, 34.09; H, 3.25; N, 3.61. Found: C, 33.30/33.29; H, 3.42/3.32; N, 3.44/3.40.

$[(\text{Bu}_2\text{Ar}^{\text{H}})\text{PtMe}(\text{CO})]^+[\text{BF}_4]^-$ (**9a**). **9a** was synthesized similarly from **6a** (10 mg, 0.015 mmol) and an aqueous solution of HBF₄ (2 μL , 0.015 mmol) in 3 mL of TFE. 5.2 mg of orange powder was obtained (47%). The product contained a small amount of TFE, which was hard to remove. ${}^1\text{H}$ NMR (500 MHz, CD_2Cl_2): $\delta = 1.14$ (t, 3H, ${}^2J_{\text{Pt-H}} = 69$ Hz, Pt-CH₃), 1.37, 1.39 (s, 18H each, C(CH₃)₃), 7.12 (d, ${}^4J_{\text{H-H}} = 1.5$ Hz, 2H, *o*-Ar-H), 7.44 (d, ${}^4J_{\text{H-H}} = 1.5$ Hz, 2H, *o*-Ar-H), 7.59 (t, ${}^4J_{\text{H-H}} = 1.5$ Hz, 1H, *p*-Ar-H), 7.64 (t, ${}^4J_{\text{H-H}} = 1.5$ Hz, 1H, *p*-Ar-H), 9.04 (t, ${}^3J_{\text{Pt-H}} = 74$ Hz, N=C-H), 9.29 (t, ${}^3J_{\text{Pt-H}} = 38$ Hz, N=C-H). ${}^{13}\text{C}$ { ${}^1\text{H}$ } NMR (125 MHz, CD_2Cl_2): $\delta = -8.81$ (Pt-CH₃), 31.10, 31.14 (C(CH₃)₃), 35.44, 35.45 (C(CH₃)₃), 117.20, 117.33,

124.80, 126.91, 153.20, 154.04, 163.40, 176.49 (Ar–C). Could not find CO resonance and two ArC resonances. IR (CH₂Cl₂): $\nu(\text{CO}) = 2108.8 \text{ cm}^{-1}$. Anal. Calcd for C₃₂H₄₇N₂O₂PtBF₄: C, 50.73; H, 6.25; N, 3.70. Found: C, 47.67/47.62; H, 5.94/5.91; N, 3.45/3.36.

[(^{OMe}Ar^HDAB^H)PtMe(CO)]⁺[BF₄][−] (**9b**). **9b** was synthesized similarly from **6b** (13.8 mg, 0.023 mmol) and an aqueous solution of HBF₄ (3 μL , 0.023 mmol) in 3 mL of TFE. 5.2 mg of a deep reddish purple powder was obtained (33%). The product contained a small amount of TFE, which was hard to remove. ¹H NMR (500 MHz, CD₂Cl₂): $\delta = 1.24$ (t, 3H, ²J_{Pt–H} = 66 Hz, Pt–CH₃), 3.84, 3.88 (s, 3H, *p*-OCH₃), 3.89, 3.94 (s, 6H each, OCH₃), 6.56, 6.90 (s, 2H each, Ar–H), 8.98, 9.21 (s, 1H each, N=C–H). IR (CH₂Cl₂): $\nu(\text{CO}) = 2110.3 \text{ cm}^{-1}$. The compound slowly decomposes in methylene chloride. ESMS. Calcd for C₂₂H₂₇N₂O₂Pt [M]⁺: 625.1445 (¹⁹⁴Pt), 626.1469 (¹⁹⁵Pt), 627.1477 (¹⁹⁶Pt). Found: 625.1447, 626.1460, 627.1473.

[(^{OMe}CF₃Ar^HDAE)PtMe(CO)]⁺[BF₄][−] (**9c**). **9c** was synthesized similarly from **6c** (14.5 mg, 0.023 mmol) and an aqueous solution of HBF₄ (3 μL , 0.023 mmol) in 3 mL of TFE. 6.0 mg of product was obtained (37%). The product contained a small amount of TFE, which was hard to remove. ¹H NMR (CD₂Cl₂): $\delta = 1.17$ (t, 3H, ²J_{Pt–H} = 68 Hz, Pt–CH₃), 3.94, 3.97 (s, 3H each, OCH₃), 7.12, 7.17, 7.32, 7.35, 7.40, 7.43 (broad s, 1H each, Ar–H), 9.10 (t, 1H, ³J_{Pt–H} = 71 Hz, N=C–H), 9.32 (t, 1H, ³J_{Pt–H} = 39 Hz, N=C–H). IR (CH₂Cl₂): $\nu(\text{CO}) = 2116.0 \text{ cm}^{-1}$. The compound quickly decomposes in methylene chloride.

Synthesis and Characterization of Methyl Aquo/Solvento Cations (10–12). The aquo/solvento adducts of **10–12** were prepared similarly to procedures described by Tilsted and co-workers.¹¹ The isolated orange/brown solids inevitably contained 5–15% decomposition products (mostly the μ -OH dimer). The amount of the impurities can be minimized by strict control of the temperature at which TFE is removed. These impurities are inert under conditions where benzene was activated and are not expected to affect the outcome of intermolecular/intramolecular competition reactions. For most kinetic studies, cations **10–12** are generated in situ (vide infra), and the chemical shifts reported below are for solutions in TFE-*d*₃ (300 and 500 MHz) in the absence of substrates unless otherwise stated. The Pt–CH₂D resonances are typically 0.01–0.02 ppm upfield of those of the corresponding Pt–CH₃ peaks. ²J_{Pt–H} can only be observed on the 300 MHz NMR instrument. Addition of benzene can significantly change the chemical shifts for the backbone methyl or H resonances.

10ai: $\delta = 0.77$ (s, 3H, ²J_{Pt–H} = 66 Hz, Pt–CH₃), 1.465, 1.48 (s, 18H each, C(CH₃)₃), 1.88, 2.03 (s, 3H each, N=C–CH₃), 3.75, 3.76 (s, 3H each, OCH₃), 6.92, 7.10 (s, 2H each, Ar–H).

10aii: $\delta = 0.765$ (s, 3H, ²J_{Pt–H} = 66 Hz, Pt–CH₃), 1.465, 1.49 (s, 18H each, C(CH₃)₃), 1.79, 2.01 (s, 3H each, N=C–CH₃), 3.75, 3.78 (s, 3H each, OCH₃), 6.91, 7.15 (s, 2H each, Ar–H).

10bi: $\delta = 0.733$ (s, 3H, ²J_{Pt–H} = 69 Hz, Pt–CH₃), 1.35, 1.36 (s, 18H each, C(CH₃)₃), 1.85, 2.01 (s, 3H each, N=C–CH₃), 6.84 (d, ⁴J_{H–H} = 1.5 Hz, 2H, *o*-Ar–H), 7.03 (d, ⁴J_{H–H} = 1.5 Hz, 2H, *o*-Ar–H), 7.53, 7.61 (t, 1H each, *p*-Ar–H).

10bii: $\delta = 0.723$ (s, 3H, ²J_{Pt–H} = 69 Hz, Pt–CH₃), 1.35, 1.37 (s, 18H each, C(CH₃)₃), 1.77, 1.99 (s, 3H each, N=C–CH₃), 6.83 (d, ⁴J_{H–H} = 1.5 Hz, 2H, *o*-Ar–H), 7.07 (d, ⁴J_{H–H} = 1.5 Hz, 2H, *o*-Ar–H), 7.52, 7.59 (t, 1H each, *p*-Ar–H).

10ci: $\delta = 0.93$ (s, 3H, ²J_{Pt–H} = Hz, Pt–CH₃), 1.97, 2.075 (s, 3H each, N=C–CH₃), 3.90–3.92 (OCH₃, cannot be identified with certainty because of overlapping with solvent peaks), 6.37, 6.50 (s, 2H each, Ar–H).

10cii: $\delta = 0.91$ (s, 3H, ²J_{Pt–H} = Hz, Pt–CH₃), 1.86, 2.08 (s, 3H each, N=C–CH₃), 3.90–3.92 (OCH₃, cannot be identified with certainty due to overlapping solvent peaks), 6.36, 6.52 (s, 2H each, Ar–H).

10di: $\delta = 0.875$ (s, 3H, ²J_{Pt–H} = Hz, Pt–CH₃), 1.95, 2.08 (s, 3H each, N=C–CH₃), 3.89–3.94 (cannot be identified with certainty due

to overlapping solvent peaks, OCH₃), 6.82, 6.95, 7.08, 7.28 (overlapping with **10dii**).

10dii: $\delta = 0.860$ (s, 3H, ²J_{Pt–H} = Hz, Pt–CH₃), 1.825, 2.05 (s, 3H each, N=C–CH₃), 3.93, 3.94 (s, 3H each, OCH₃), 6.82, 6.93, 6.97, 7.08 (broad s, 1H, Ar–H), 7.26 (broad s, 2H total, Ar–H, split into two peaks in the presence of benzene).

11ai: $\delta = 0.66$ (s, 3H, ²J_{Pt–H} = 72 Hz, Pt–CH₃), 1.74, 1.89 (s, 3H each, N=C–CH₃), 2.15, 2.29 (s, 6H each, *o*-Ar–CH₃), 2.34 (overlapping s, 6H total, *p*-Ar–CH₃), 7.06, 7.11 (s, 4H total, Ar–H). (In the presence of 100 μL of C₆D₆): $\delta = 0.74$ (s, 3H, ²J_{Pt–H} = 72 Hz, Pt–CH₃), 1.58, 1.73 (s, 3H each, N=C–CH₃), 2.16, 2.27 (s, 6H each, *o*-Ar–CH₃), 2.36, 2.38 (s, 3H each, *p*-Ar–CH₃), 7.05, 7.10 (s, 4H total, Ar–H).

11aii: $\delta = 0.64$ (s, 3H, ²J_{Pt–H} = 72 Hz, Pt–CH₃), 0.63 (s, Pt–CH₂D), 1.63, 1.81 (s, 3H each, N=C–CH₃), 2.15, 2.26 (s, 6H each, *o*-Ar–CH₃), 2.34 (overlapping s, 6H total, *p*-Ar–CH₃), 7.06, 7.10 (s, 4H total, Ar–H). (In the presence of 100 μL of C₆D₆): $\delta = 0.73$ (s, 3H, ²J_{Pt–H} = 72 Hz, Pt–CH₃), 0.72 (s, Pt–CH₂D), 1.48, 1.66 (s, 3H each, N=C–CH₃), 2.16, 2.27 (s, 6H each, *o*-Ar–CH₃), 2.36, 2.38 (s, 3H each, *p*-Ar–CH₃), 7.05, 7.10 (s, 4H total, Ar–H).

11bi: $\delta = 0.66$ (s, 3H, ²J_{Pt–H} = 72 Hz, Pt–CH₃), 1.77, 1.92 (s, 3H each, N=C–CH₃), 2.21, 2.35 (s, 6H each, *o*-Ar–CH₃), 7.24–7.28 (m, 6H total, Ar–H).

11bii: $\delta = 0.64$ (s, 3H, ²J_{Pt–H} = 72 Hz, Pt–CH₃), 0.62 (s, Pt–CH₂D), 1.65, 1.83 (s, 3H each, N=C–CH₃), 2.21, 2.32 (s, 6H each, *o*-Ar–CH₃), 7.24–7.28 (m, 6H total, Ar–H).

11ci: $\delta = 0.70$ (s, 3H, ²J_{Pt–H} = 72 Hz, Pt–CH₃), 1.78, 1.91 (s, 3H each, N=C–CH₃), 2.18, 2.30 (s, 6H each, *o*-Ar–CH₃), 7.46 (s, 4H total, Ar–H).

11cii: $\delta = 0.69$ (s, 3H, ²J_{Pt–H} = 72 Hz, Pt–CH₃), 0.67 (s, Pt–CH₂D), 1.65, 1.84 (s, 3H each, N=C–CH₃), 2.18, 2.27 (s, 6H each, *o*-Ar–CH₃), 7.43 (s, 4H total, Ar–H). (In the presence of 100 μL of C₆D₆): $\delta = 0.73$ (s, 3H, ²J_{Pt–H} = 72 Hz, Pt–CH₃), 1.46, 1.66 (s, 3H each, N=C–CH₃), 2.13, 2.24 (s, 6H each, *o*-Ar–CH₃), 7.42 (s, 4H total, Ar–H).

12ai: $\delta = 1.25$ (br s, 3H, Pt–CH₃), 1.38, 1.40 (s, 18H each, C(CH₃)₃), 7.13 (d, ⁴J_{H–H} = 1.5 Hz, 2H, *o*-Ar–H), 7.34 (d, ⁴J_{H–H} = 1.5 Hz, 2H, *o*-Ar–H), 7.66 (t, ⁴J_{H–H} = 1.5 Hz, 1H, *p*-Ar–H), 7.77 (t, ⁴J_{H–H} = 1.5 Hz, 1H, *p*-Ar–H), 8.69 (s, 1H, N=C–H), 8.71 (s, 1H, N=C–H). (In the presence of 30 μL of C₆D₆): $\delta = 1.29$ (br s, 3H, Pt–CH₃), 1.42, 1.44 (s, 18H each, C(CH₃)₃), 7.16 (d, ⁴J_{H–H} = 1.5 Hz, 2H, *o*-Ar–H), 7.53 (d, ⁴J_{H–H} = 1.5 Hz, 2H, *o*-Ar–H), 7.70 (t, ⁴J_{H–H} = 1.5 Hz, 1H, *p*-Ar–H), 7.83 (t, ⁴J_{H–H} = 1.5 Hz, 1H, *p*-Ar–H), 8.39 (s, 1H, N=C–H), 8.43 (s, 1H, N=C–H).

12aii: $\delta = 1.24$ (br s, 3H, Pt–CH₃), 1.38, 1.41 (s, 18H each, C(CH₃)₃), 7.13 (d, ⁴J_{H–H} = 1.5 Hz, 2H, *o*-Ar–H), 7.51 (d, ⁴J_{H–H} = 1.5 Hz, 2H, *o*-Ar–H), 7.65 (t, ⁴J_{H–H} = 1.5 Hz, 1H, *p*-Ar–H), 7.77 (t, ⁴J_{H–H} = 1.5 Hz, 1H, *p*-Ar–H), 8.80 (br s, 1H, N=C–H), 8.85 (s, 1H, N=C–H). (In the presence of 30 μL of C₆D₆): $\delta = 1.27$ (br s, 3H, Pt–CH₃), 1.42, 1.44 (s, 18H each, C(CH₃)₃), 7.12 (d, ⁴J_{H–H} = 1.5 Hz, 2H, *o*-Ar–H), 7.49 (d, ⁴J_{H–H} = 1.5 Hz, 2H, *o*-Ar–H), 7.68 (t, ⁴J_{H–H} = 1.5 Hz, 1H, *p*-Ar–H), 7.81 (t, ⁴J_{H–H} = 1.5 Hz, 1H, *p*-Ar–H), 8.53 (br s, 1H, N=C–H), 8.55 (s, 1H, N=C–H).

12bii: (In the presence of 30 μL of C₆D₆): $\delta = 1.40$ (br s, 3H, Pt–CH₃), 1.38 (s, Pt–CH₂D), 3.88, 3.94 (s, 3H each, *p*-OCH₃), 3.90, 3.96 (s, 6H each, *o*-OCH₃), 6.59, 6.97 (s, 2H each, Ar–H), 8.71, 8.80 (s, 1H each, N=C–H).

12cii: $\delta = 1.34$ (br s, 3H, Pt–CH₃), 1.33 (s, Pt–CH₂D), 3.91, 3.94 (s, 3H each, OCH₃), 7.03, 7.15, 7.31, 7.35, 7.38, 7.48 (broad s, 1H each, Ar–H), 8.96, 9.07 (s, 1H each, N=C–H). (In the presence of 30 μL of C₆D₆): $\delta = 1.37$ (br s, 3H, Pt–CH₃), 1.36 (s, Pt–CH₂D), 3.94, 3.97 (s, 3H each, OCH₃), 7.03, 7.15, 7.31, 7.35, 7.38, 7.48 (broad s, 1H each, Ar–H), 8.75, 8.84 (s, 1H each, N=C–H).

Syntheses of Methyl-Acetonitrile Cations (13–15). Acetonitrile adducts **13–15** were synthesized according to procedures reported in

ref 11. Without added acetonitrile, **13–15** are in equilibrium with solvento adducts in CD₃OD, CD₃CD₂OD, and (CD₃)₂CDOD. ¹H NMR data follows.

13b (TFE-*d*₃): $\delta = 0.682$ (s, 3H, ²J_{Pt-H} = 72 Hz, Pt-CH₃), 1.36, 1.39 (s, 18H each, C(CH₃)₃), 1.92 (s, 3H, NC-CH₃), 1.99, 2.02 (s, 3H each, N=C-CH₃), 6.84 (d, ⁴J_{H-H} = 1.5 Hz, 2H, *o*-Ar-H), 6.97 (d, ⁴J_{H-H} = 1.5 Hz, 2H, *o*-Ar-H), 7.56, 7.60 (t, 1H each, *p*-Ar-H).

13b (CD₃OD): $\delta = 0.55$ (s, 3H, ²J_{Pt-H} = 73 Hz, Pt-CH₃), 1.37, 1.41 (s, 18H each, C(CH₃)₃), 2.05, 2.08 (s, 3H each, N=C-CH₃), 2.14 (s, 3H, NC-CH₃), 6.91 (d, ⁴J_{H-H} = 1.5 Hz, 2H, *o*-Ar-H), 7.05 (d, ⁴J_{H-H} = 1.5 Hz, 2H, *o*-Ar-H), 7.47, 7.52 (t, 1H each, *p*-Ar-H).

13b (CD₃CD₂OD): $\delta = 0.56$ (s, 3H, ²J_{Pt-H} = 75 Hz, Pt-CH₃), 1.37, 1.41 (s, 18H each, C(CH₃)₃), 2.09, 2.12 (s, 3H each, N=C-CH₃), 2.17 (s, 3H, NC-CH₃), 6.93 (d, ⁴J_{H-H} = 1.5 Hz, 2H, *o*-Ar-H), 7.06 (d, ⁴J_{H-H} = 1.5 Hz, 2H, *o*-Ar-H), 7.44, 7.49 (t, 1H each, *p*-Ar-H).

13b ((CD₃)₂CDOD): $\delta = 0.59$ (s, 3H, ²J_{Pt-H} = 75 Hz, Pt-CH₃), 1.37, 1.41 (s, 18H each, C(CH₃)₃), 2.12, 2.15 (s, 3H each, N=C-CH₃), 2.19 (s, 3H, NC-CH₃), 6.94 (d, ⁴J_{H-H} = 1.5 Hz, 2H, *o*-Ar-H), 7.08 (d, ⁴J_{H-H} = 1.5 Hz, 2H, *o*-Ar-H), 7.42, 7.46 (t, 1H each, *p*-Ar-H).

13d (TFE-*d*₃): $\delta = 0.76$ (t, 3H, ²J_{Pt-H} = 67 Hz, Pt-CH₃), 2.01, 2.09 (s, 3H each, N=C-CH₃), 2.07 (s, 3H, NC-CH₃), 3.90, 3.92 (s, 3H each, OCH₃), 6.78, 6.88, 6.89, 7.05, 7.24, 7.26 (broad s, 1H each, Ar-H).

13d (CD₃OD): $\delta = 0.61$ (t, 3H, ²J_{Pt-H} = 67 Hz, Pt-CH₃), 2.09, 2.15 (s, 3H each, N=C-CH₃), 2.27 (s, 3H, NC-CH₃), 3.94, 3.97 (s, 3H each, OCH₃), 6.95, 7.00, 7.07, 7.15, 7.27, 7.31 (broad s, 1H each, Ar-H).

14b (CD₃OD): $\delta = 0.44$ (s, 3H, ²J_{Pt-H} = 75 Hz, Pt-CH₃), 2.01, 2.05 (s, 3H each, N=C-CH₃), 2.06 (s, 3H, NC-CH₃), 2.23, 2.34 (s, 6H each, Ar-CH₃), 7.25–7.34 (m, 6H total, Ar-H).

14c (TFE-*d*₃): $\delta = 0.62$ (s, 3H, ²J_{Pt-H} = 75 Hz, Pt-CH₃), 1.88, 1.94 (s, 3H each, N=C-CH₃), 1.97 (s, 3H, NC-CH₃), 2.15, 2.26 (s, 6H each, Ar-CH₃), 7.42, 7.47 (s, 2H each, Ar-H).

14c (CD₃OD): $\delta = 0.48$ (s, 3H, ²J_{Pt-H} = 75 Hz, Pt-CH₃), 2.03, 2.06 (s, 3H each, N=C-CH₃), 2.19 (s, 3H, NC-CH₃), 2.21, 2.33 (s, 6H each, Ar-CH₃), 7.48, 7.53 (s, 2H each, Ar-H).

NMR Data for (μ-OH)₂ Dimer 16b. ¹H NMR (TFE-*d*₃): 1.24 (s, 36H, C(CH₃)₃), 1.91 (s, 6H each, N=C-CH₃), 5.30 (br s, O-H), 7.03 (d, ⁴J_{H-H} = 1.5 Hz, 4H, *o*-Ar-H), 7.60 (t, ⁴J_{H-H} = 1.5 Hz, 4H, *p*-Ar-H). ¹⁹F NMR (TFE-*d*₃): -152.0 (BF₄⁻).

Measurement of Kinetics for C–H Bond Activation of Aromatic Substrates. Dry TFE-*d*₃ was vacuum transferred into an oven-dried 5 mm thin-walled NMR tube with J-Young valve. Approximately 0.0076 mmol of (N–N)PtMe₂ (**4–6**), 1 μL of aqueous HBF₄ (48 wt %, 0.00765 mmol), and a predetermined amount of D₂O were then added to the tube. The mixture was shaken to form a clear solution. ¹H NMR spectra were then taken of the mixture to ensure clean conversion to aquo/solvento adducts **10–12**. A predetermined amount of substrate was then added to the NMR tube, and after allowing the mixture to equilibrate to the preset temperature in the probe, disappearance of the starting material (and appearance of the products **17–19**) was monitored. Probe temperatures were calibrated with a methanol thermometer and were maintained at ±0.2 °C throughout data acquisition. The observed rate constants are calculated by curve fitting to the expression $A_t = A_f + (A_0 - A_f) \times \exp(-k_{\text{obs}}t)$, where A_t is the area under the peak (or the peak height). The area under the peak is found by multiplying the peak height by the full width at half maximum. The volume of the reaction mixture is determined as V (mL) = 0.01384*H* - 0.006754, where *H* is the solvent height in millimeters. The water concentration is calculated as follows: $[\text{H}_2\text{O}] = [(1 \mu\text{L} \times 1.4 \text{ g mL}^{-1} \times 52\% + y \mu\text{L} \times 1 \text{ g mL}^{-1})/18 \text{ g mol}^{-1} - 0.00765 \times n/(n+1)]/V$ (mL), where 1.4 g mL⁻¹ is the density of the aqueous HBF₄ solution, 52% is the wt % of water in this aqueous solution, *y* is the amount of extra water added, 1 g mL⁻¹ is the density of water, and *n* is the ratio of aquo:solvento adducts. The chemical shifts for the phenyl complexes **17–19** reported below were measured in TFE in the presence of benzene. Addition of

a small amount of benzene (e.g., 15 μL) to TFE-*d*₃ shifts the resonances for the diimine backbone methyls or protons by as much as 0.3 ppm and can significantly affect shimming.

17ai: $\delta = 1.34, 1.51$ (s, 18H each, C(CH₃)₃), 1.94, 2.12 (s, 3H each, N=C-CH₃), 3.57, 3.77 (s, 3H each, OCH₃), 7.19, 7.75 (s, 2H each, Ar-H), resonances for Ph-H's cannot be identified with certainty.

17aii: $\delta = 1.33, 1.51$ (s, 18H each, C(CH₃)₃), 1.88, 2.14 (s, 3H each, N=C-CH₃), 3.59, 3.80 (s, 3H each, OCH₃), 6.71, 7.25 (s, 2H each, Ar-H), 6.73 (m, 1H, Ph-H_p), 6.79 (t, 7.4 Hz, 2H, Ph-H_o), 6.87 (m, 2H, Ph-H_m).

17bi: $\delta = 1.23, 1.40$ (s, 18H each, C(CH₃)₃), 1.90, 2.10 (s, 3H each, N=C-CH₃), 6.61 (d, ⁴J_{H-H} = 1.5 Hz, 2H, *o*-Ar-H), 7.14 (d, ⁴J_{H-H} = 1.5 Hz, 2H, *o*-Ar-H), 7.23, 7.68 (t, 1H each, *p*-Ar-H), resonances for Ph-H's cannot be identified with certainty.

17bii: $\delta = 1.22, 1.41$ (s, 18H each, C(CH₃)₃), 1.85, 2.14 (s, 3H each, N=C-CH₃), 6.61 (d, ⁴J_{H-H} = 1.5 Hz, 2H, *o*-Ar-H), 7.18 (d, ⁴J_{H-H} = 1.5 Hz, 2H, *o*-Ar-H), 7.26, 7.65 (t, 1H each, *p*-Ar-H), 6.68 (m, 1H, Ph-H_p), 6.73 (m, 2H, Ph-H_o), 6.82 (m, 2H, Ph-H_m).

17ci: $\delta = 2.04, 2.19$ (s, 3H each, N=C-CH₃), 3.68, 3.89 (s, 3H each, *p*-OCH₃), 3.72, 3.922 (s, 6H each, *o*-OCH₃), 6.09, 6.55 (s, 2H each, Ar-H), resonances for Ph-H's cannot be identified with certainty.

17cii: $\delta = 1.97, 2.19$ (s, 3H each, N=C-CH₃), 3.71, 3.90 (s, 3H each, *p*-OCH₃), 3.70, 3.915 (s, 6H each, *o*-OCH₃), 6.08, 6.67 (s, 2H each, Ar-H), 6.80 (m, 1H, Ph-H_p), 6.86 (tt, 8 Hz, 1.8 Hz, 2H, Ph-H_o), 6.94 (m, 2H, Ph-H_m).

17di: $\delta = 2.00, 2.16$ (s, 3H each, N=C-CH₃), 3.70, 3.92 (s, 3H each, OCH₃), 6.48, 6.67, 6.90, 7.00, 7.30, 7.37 (broad s, 1H, Ar-H), resonances for Ph-H's cannot be identified with certainty.

17dii: $\delta = 1.90, 2.15$ (s, 3H each, N=C-CH₃), 3.67, 3.92 (s, 3H each, OCH₃), 6.46, 6.70, 6.91, 7.02, 7.28, 7.37 (broad s, 1H, Ar-H), 6.74 (m, 1H, Ph-H_p), 6.79 (t, 9 Hz, 2H, Ph-H_o), 6.85 (m, 2H, Ph-H_m).

18ai: $\delta = 1.69, 1.87$ (s, 3H each, N=C-CH₃), 2.13, 2.35 (s, 6H each, *o*-Ar-CH₃), 2.15, 2.37 (s, 3H each, *p*-Ar-CH₃), 6.69, 7.14 (s, 4H total, Ar-H), 6.69–6.84 (m, 5H, Ph-H's).

18aii: $\delta = 1.61, 1.81$ (s, 3H each, N=C-CH₃), 2.11, 2.35 (s, 6H each, *o*-Ar-CH₃), 2.17, 2.39 (s, 3H each, *p*-Ar-CH₃), 6.72, 7.13 (s, 4H total, Ar-H), 6.69–6.84 (m, 5H, Ph-H's).

18bi: $\delta = 1.75, 1.96$ (s, 3H each, N=C-CH₃), 2.20, 2.42 (s, 6H each, *o*-Ar-CH₃), aryl peaks cannot be identified with certainty (many overlapping peaks).

18bii: $\delta = 1.67, 1.89$ (s, 3H each, N=C-CH₃), 2.18, 2.40 (s, 6H each, *o*-Ar-CH₃), 6.91, 7.30 (s, 2H each, *o*-Ar-H), 6.93, 7.29 (s, 1H each, *p*-Ar-H), 6.72–7.00 (m, 5H, Ph-H's).

18ci: $\delta = 1.77, 1.95$ (s, 3H each, N=C-CH₃), 2.14, 2.36 (s, 6H each, *o*-Ar-CH₃), 7.03, 7.48 (s, 4H total, Ar-H), 6.69–6.84 (m, 5H, Ph-H's).

18cii: $\delta = 1.67, 1.89$ (s, 3H each, N=C-CH₃), 2.12, 2.34 (s, 6H each, *o*-Ar-CH₃), 7.06, 7.46 (s, 2H each, Ar-H), 6.69–6.90 (m, 5H, Ph-H's).

19aii: $\delta = 1.23, 1.46$ (s, 18H each, C(CH₃)₃), 6.810 (d, ⁴J_{H-H} = 1.5 Hz, 2H, *o*-Ar-H), 7.52 (d, ⁴J_{H-H} = 1.5 Hz, 2H, *o*-Ar-H), 7.45 (t, ⁴J_{H-H} = 1.5 Hz, 1H, *p*-Ar-H), 7.84 (t, ⁴J_{H-H} = 1.5 Hz, 1H, *p*-Ar-H), 8.46 (br s, 1H, N=C-H), 8.53 (s, 1H, N=C-H), 6.84 (m, 2H, Ph-H_o). The other three Ph-H peaks are probably hidden by free benzene peaks.

19bii: $\delta = 3.78, 3.95$ (s, 3H each, *p*-OCH₃), 3.65, 3.97 (s, 6H each, *o*-OCH₃), 6.29, 6.99 (s, 2H each, Ar-H), 8.66, 8.79 (s, 1H each, N=C-H), 7.06–7.14 (m, Ph-H's).

19cii: (In the presence of 30 μL of C₆H₆), $\delta = 3.61, 3.94$ (s, 3H each, OCH₃), 6.62, 6.87, 7.08, 7.35, 7.44, 7.48 (broad s, 1H each, Ar-H), 8.68, 6.82 (s, 1H each, N=C-H), cannot be identified with certainty. (In the presence of 60 μL of C₆D₆): $\delta = 3.60, 3.93$ (s, 3H

each, OCH₃), 6.62, 6.87, 7.08, 7.35, 7.44, 7.48 (broad s, 1H each, Ar-H), 8.53, 8.66 (s, 1H each, N=C-H), cannot be identified with certainty.

20bii: δ = 1.16, 1.24 (s, 9H each, C(CH₃)₃), 1.39 (s, 18H, C(CH₃)₃), 1.74, 2.08 (s, 3H each, N=C-CH₃), 1.99, 2.51 (s, 3H each, *p*-xylene-Me), 6.55 (t, ⁴J_{H-H} = 1.8 Hz, 1H, *o*-Ar-H), 6.64 (t, ⁴J_{H-H} = 1.8 Hz, 1H, *o*-Ar-H), 7.19 (d, 2H, *o*-Ar-H), 7.23, 7.64 (t, ⁴J_{H-H} = 1.8 Hz, 1H each, *p*-Ar-H), 6.43 (m, 1H, *p*-xylene-H), 6.55 (m, 2H, *p*-xylene-H).

20bi: δ = 1.20, 1.21 (s, 9H each, C(CH₃)₃), 1.39 (s, 18H, C(CH₃)₃), 1.86, 1.98 (s, 3H each, N=C-CH₃), 2.13, 2.38 (s, 3H each, *p*-xylene-Me), 6.67 (m, 2H, *o*-Ar-H), 7.05 (d, ⁴J_{H-H} = 1.5 Hz, 2H, *o*-Ar-H), 7.23, 7.56 (t, ⁴J_{H-H} = 1.8 Hz, 1H each, *p*-Ar-H), 6.25 (m, 1H, *p*-xylene-H), 6.60 (m, 2H, *p*-xylene-H).

20b: (MeCN adduct in CD₃NO₂), δ = 1.16, 1.28 (s, 9H each, C(CH₃)₃), 1.43 (s, 18H, C(CH₃)₃), 1.95 (s, 3H, N=C-CH₃), 2.02 (s, 3H, CH₃CN), 2.17, 2.27, 2.40 (s, 3H each, N=C-CH₃ or *p*-xylene-Me), 6.36 (m, 1H, *p*-xylene-H), 6.50 (m, 2H, *p*-xylene-H), 6.36 (t, ⁴J_{H-H} = 1.8 Hz, 1H, *o*-Ar-H), 6.77 (t, ⁴J_{H-H} = 1.5 Hz, 1H, *o*-Ar-H), 7.16 (d, 2H, *o*-Ar-H), 7.24 (t, ⁴J_{H-H} = 1.5 Hz, 1H, *p*-Ar-H), 7.63 (t, ⁴J_{H-H} = 1.8 Hz, 1H, *p*-Ar-H).

21b: (MeCN adduct in CD₃NO₂), δ = 1.34, 1.38 (s, 18 H each, C(CH₃)₃), 1.75 (t, ³J_{H-H} = 27 Hz, 3H, CH₃CN), 2.081, 2.135 (s, 3H, N=C-CH₃), 2.15 (s, 6H, mesitylene-Me), 2.80 (t, ²J_{H-H} = 103 Hz, 2H, Pt-CH₂Ar), 6.51 (m, 2H, mesitylene-H), 6.59 (m, 1H, mesitylene-H), 6.93, 6.97 (d, ⁴J_{H-H} = 1.5 Hz, 2H each, *o*-Ar-H), 7.40, 7.48 (t, ⁴J_{H-H} = 1.5 Hz, 1H each, *p*-Ar-H).

21bii: (Aquo adduct in TFE-*d*₃), δ = 1.38, 1.42 (s, 18H each, C(CH₃)₃), 1.78, 1.92 (s, 3H, N=C-CH₃), 2.53 (s, 6H, mesitylene-Me), 5.93 (br s, 2H, *o*-mesitylene-H, substantial H incorporation into this position when mesitylene-*d*₁₂ is used), 6.47, 7.06 (d, ⁴J_{H-H} = 1.5 Hz, 2H each, *o*-Ar-H), 7.56, 7.60 (t, ⁴J_{H-H} = 1.5 Hz, 1H each, *p*-Ar-H), several peaks cannot be identified with certainty; they are probably buried under free mesitylene peaks.

22bii: Most peaks cannot be identified with certainty, except 1.23 (s, C(CH₃)₃) and 1.70, 2.07 (s, N=C-CH₃).

Measurement of Equilibrium Constants. Dry TFE-*d*₃ was vacuum transferred into an oven-dried J-Young tube. Approximately 0.0076 mmol of (N-N)PtMe₂ (**4-6**) and 1 μ L of aqueous HBF₄ (48 wt %, 0.00765 mmol) were then added to the tube. After allowing the mixture to equilibrate to 20 °C, the ratio of the aquo to solvento adducts, *n*, was then determined by integration. The water concentration was determined as follows: [(1 μ L \times 1.4 g mL⁻¹ \times (1-0.48))/18 g mol⁻¹] - 0.0076 mmol \times *n*/(1 + *n*)/*V* (mL). Volume was determined as described above. The TFE-*d*₃ concentration was taken as 14.07 M.

Acetonitrile Exchange Reactions. To an oven-dried NMR tube was added 3.5 mg of the appropriate acetonitrile adduct **13-15** (2.5 mg in (CD₃)₂CDOD because of limited solubility). About 0.7 mL of the deuterated solvent was then added, and a ¹H NMR spectrum was recorded before addition of a predetermined amount of CD₃CN. Under these conditions, the acetonitrile adducts were the only observable species in solution. After allowing the mixture to equilibrate to a preset temperature (~5 min), the disappearance of coordinated CH₃CN and the appearance of free CH₃CN were monitored, and the observed rate of exchange was determined from the following expression: $A_t = A_f + (A_0 - A_f) \times \exp(-k_{\text{ext}}t)$, where A_t is the area under the peak (or the peak height). The volume of the solution is determined as described above.

Measurement of KIE via Inter- or Intramolecular Competition Reactions. Dry TFE-*d*₃ was added to an oven-dried NMR tube containing preformed aquo/solvento adducts **10**. A mixture of 1:1 C₆H₆:C₆D₆ or C₆D₃H₃ was then added to the tube. After the reaction was complete, the integration ratio of CH_{*n*}D_{4-*n*}:CH₄ was then taken to give the KIE.

Measurement of the Ratio of CH₃D to CH₄ as a Function of Added Acetonitrile in the Protonolysis of **4b.** To a suspension of 0.0076 mol of **4b** over dry TFE-*d*₃ in oven-dried NMR tube was added a predetermined amount of CD₃CN. To this mixture, 5 μ L of a stock solution of 1 μ L of aqueous HBF₄ (48 wt %) in 24 μ L of TFE-*d*₃ was added. The tube was shaken, and after a clear orange solution was formed, the ratio of CH₃D:CH₄ was measured by integration. To account for the percentage of protonolysis by H⁺ (rather than D⁺), the H⁺ concentration was measured by integrating the [OH] resonance against the aromatic protons of **4b**. H⁺ typically accounts for 1-3% of the total H⁺/D⁺ source. This percentage was subtracted from the percentage of liberated CH₄. The adjusted ratio of CH₃D:CH₄ was then plotted against the acetonitrile concentrations to yield Figure 1.

Acknowledgment. Support by the National Science Foundation (Grant No. CHE-9807496), Akzo-Nobel, and BP are gratefully acknowledged. We thank Dr. Joseph Sadighi for preparing the diimine ligand **1a** and for devising the synthetic route for the preparation of diimine ligands **3**.

Supporting Information Available: Summary of arene C-H bond activation kinetic data and derivation of the rate law for Scheme 11 (PDF). This material is available free of charge via the Internet at <http://pubs.acs.org>.

JA011189X